cmgh

ORIGINAL RESEARCH

Single-Cell Transcriptomics Reveals Zone-Specific Alterations of Liver Sinusoidal Endothelial Cells in Cirrhosis

Tingting Su,[1,2] Yilin Yang,[1] Sanchuan Lai,[1] Jain Jeong,[1] Yirang Jung,[1] Matthew McConnell,[1] Teruo Utsumi,[1] and Yasuko Iwakiri[1]

[1]Department of Internal Medicine, Section of Digestive Diseases, Yale School of Medicine, New Haven, Connecticut; and [2]Department of Gastroenterology, First Affiliated Hospital, School of Medicine, Zhejiang University, Zhejiang, China
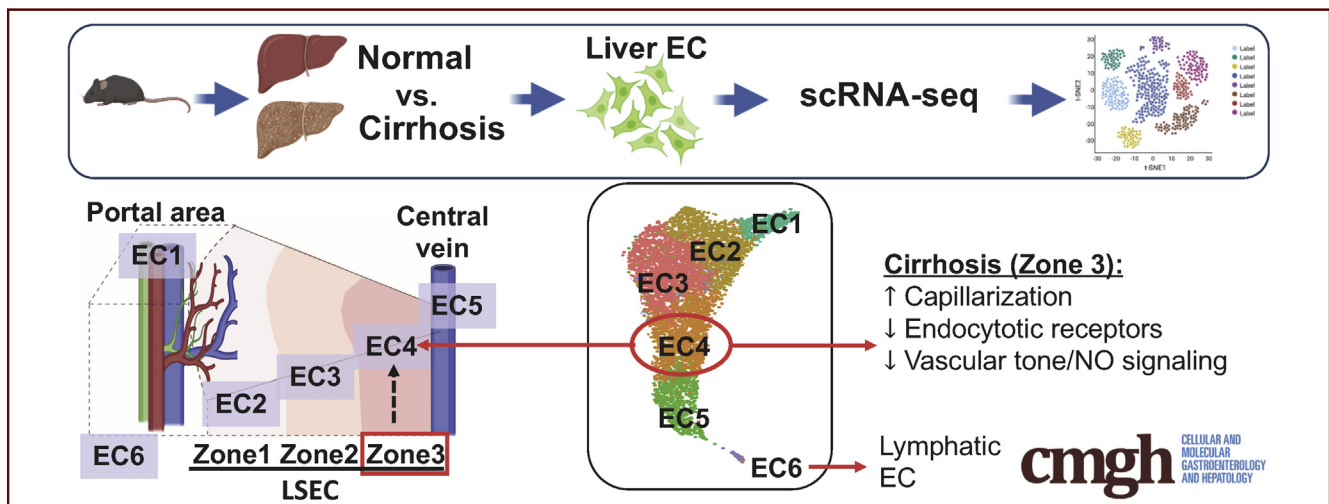
SUMMARY

We identified and mapped trascriptomic profiles of heterogeneous liver endothelial cells (ECs) in normal and cirrhotic mouse livers. Landmark genes in each EC cluster are conserved even in cirrhosis, and zone 3 liver sinusoidal ECs are most vulnerable to injury.

BACKGROUND: Dysfunction of liver sinusoidal endothelial cells (LSECs) is permissive for the progression of liver fibrosis and cirrhosis and responsible for its clinical complications. Here, we have mapped the spatial distribution of heterogeneous liver ECs in normal vs cirrhotic mouse livers and identified zone-specific transcriptomic changes of LSECs associated with liver cirrhosis using scRNA-seq technology.

APPROACH & RESULTS: Cirrhosis was generated in endothelial specific green fluorescent protein (GFP) reporter mice through carbon tetrachloride inhalation for 12 weeks. GFP-positive liver EC populations were isolated from control and cirrhotic mice by FACS. We identified 6 clusters of liver EC populations including 3 clusters of LSECs, 2 clusters of vascular ECs and 1 cluster of lymphatic ECs. Based on previously reported LSEC-landmarks, we mapped the 3 clusters of LSECs in zones 1, 2, and 3, and determined phenotypic changes in each zone between control and cirrhotic mice. We found genes representing capillarization of LSECs (eg, CD34) as well as

extracellular matrix genes were most upregulated in LSECs of zone 3 in cirrhotic mice, which may contribute to the development of basement membranes. LSECs in cirrhotic mice also demonstrated decreased expression of endocytic receptors, most remarkably in zone 3. Transcription factors (Klf2 [Kruppel-like factor-2], Klf4 [Kruppel-like factor-4], and AP-1) that induce nitric oxide production in response to shear stress were downregulated in LSECs of all zones in cirrhotic mice, implying increased intrahepatic vascular resistance.

CONCLUSION: This study deepens our knowledge of the pathogenesis of liver cirrhosis at a spatial, cell-specific level, which is indispensable for the development of novel therapeutic strategies to target the most dysfunctional liver ECs. *(Cell Mol Gastroenterol Hepatol 2021;11:1139–1161; https://doi.org/10.1016/j.jcmgh.2020.12.007)*

Liver endothelial cells (ECs), including liver sinusoidal ECs (LSECs), vascular ECs, and lymphatic ECs (LyECs), play a central role in liver homeostasis by, among other functions, regulating intrahepatic vascular tone, immune cell function, and quiescence of hepatic stellate cells (HSCs). Recent development of single-cell RNA sequencing (scRNA-seq) technology has enabled us to identify heterogeneity of these ECs, leading us to link

specific EC subpopulations to particular EC functions. Another important factor that can confer different traits to liver ECs is their spatial distributions. The liver consists of repeating anatomical units termed lobules. In each liver lobule, blood flows from the portal vein and hepatic artery toward the central vein, creating gradients of oxygen, nutrients, and hormones. In line with these graded microenvironments, key genes in hepatic cells, such as hepatocytes, HSCs, and ECs, are differentially expressed along the lobule axis, a phenomenon termed zonation.[1–4] Therefore, the roles that hepatic cells play in liver physiology and pathophysiology can be zone specific.[3] Thus, characterizing hepatic cells according to their spatial distribution is key to a complete understanding of their physiological functions.

Recognizing the importance of this type of analysis, a recent study by MacParland et al[5] revealed transcriptomic profiles of heterogeneous hepatic EC populations from healthy human donor livers using scRNA-seq technology and identified 3 EC populations, including zone 1 LSECs, zone 2 and 3 LSECs, and vascular ECs. Another recent study demonstrated the zonation patterns of liver EC genes in mice by paired-cell RNA-seq, which profiled gene expression of hepatocytes and loosely attached adjacent ECs and determined localization of the ECs in liver lobules based on expression of hepatocyte zonal landmark genes.[1] Although spatial localization was not explored, Ramachandran et al[6] performed extensive scRNA-seq analyses of all liver nonparenchymal cells, including liver ECs, isolated from human cirrhotic livers in the setting of liver transplantation, and determined detailed transcriptomic profiles that were altered in cirrhosis.

While these studies have significantly advanced our understanding of heterogeneous EC populations in normal and cirrhotic livers, further characterizations of liver EC populations are still needed to understand important questions related to liver EC biology in both normal and diseased livers. For example, it is not clear whether unique zonal profiles of liver ECs are maintained or lost in cirrhosis. How are liver EC transcriptomic profiles altered in liver cirrhosis related to LSEC phenotypes observed in cirrhosis, such as capillarization, EC dysfunction (eg, dysregulation of vascular tone) and endothelial-to-mesenchymal transition (EndMT)? What are appropriate markers to represent these phenotypic changes in LSECs? Are these phenotypic changes in LSECs zone-specific?

To address these questions and others, we performed scRNA-seq analysis of liver ECs isolated from EC-specific green fluorescent protein (GFP) reporter mice, which allowed us to enrich liver EC populations efficiently and exclusively. We first identified heterogeneous liver EC populations. Second, we determined the spatial landscape of these ECs in normal and cirrhotic livers.[1] Third, focusing on LSEC populations, we mapped 3 unique clusters of LSECs that aligned with zones 1, 2, and 3, determined transcriptomic changes of LSECs in cirrhotic livers in a zone-specific manner, and related these transcriptomic changes to known phenotypic changes of LSECs in cirrhotic livers.

Results

scRNA-seq Identified Clusters of Liver ECs in Control and Cirrhotic Mice

We performed 10x scRNA-seq analysis on liver EC–enriched populations isolated from control and cirrhotic mice (Figure 1A). All mice used were EC-specific GFP-expressing mice. GFP-positive and nonapoptotic liver ECs were selected from nonparenchymal cell fractions pooled from 3 mice per group by fluorescence-activated cell sorting (FACS) and were confirmed by a fluorescent image of GFP expression (Figure 1B). Figure 1C illustrates a workflow of data analysis. After excluding low-quality cells (expressing fewer than 200 genes or having a mitochondrial genome transcript ratio >0.2) and GFP-negative cells, 3248 cells from control mice, and 4076 cells from cirrhotic mice were used for further analysis. Our analysis identified a total of 12 clusters with similar landscapes between control and cirrhotic groups (Figure 1D). Although all the analyzed cells were positive for GFP and VE-cadherin (Cdh5) (a gene known to be expressed in all ECs) (Figure 1E), some clusters also expressed markers of hepatocytes, T cells, cholangiocytes, macrophages, and HSCs (Figure 2). Inclusion of other cell types with GFP expression could be due to adherence of ECs to those cells, which may have allowed them to be recognized as single cells during the 10x scRNA-seq analysis.[1] We excluded these clusters for further analysis and focused only on those clusters with pure EC populations, which included clusters 1–6, corresponding to EC1 to EC5 and LyECs (Figure 1F). The representative marker genes of these clusters are presented with a heatmap (Figure 1G).

Spatial Lobular Locations of Heterogeneous Liver EC Populations Were Determined

We first determined a spatial distribution of each cluster in the control (normal) mouse liver based on expression of well-known landmark genes.[1,7–9] Consistent with previous studies,[1,10] most of the EC genes analyzed exhibited spatial gradations rather than binary expression patterns without clear boundaries between different EC clusters, except for cluster 6. *Clusters 1–5 (EC1–EC5): An Atlas of LSECs and Vascular ECs (ie, Arterial and Central Venous ECs) in the Control Mouse Liver.* Because LSECs are unique ECs, we differentiated LSECs from vascular ECs such as arterial and central venous ECs, using currently known vascular and
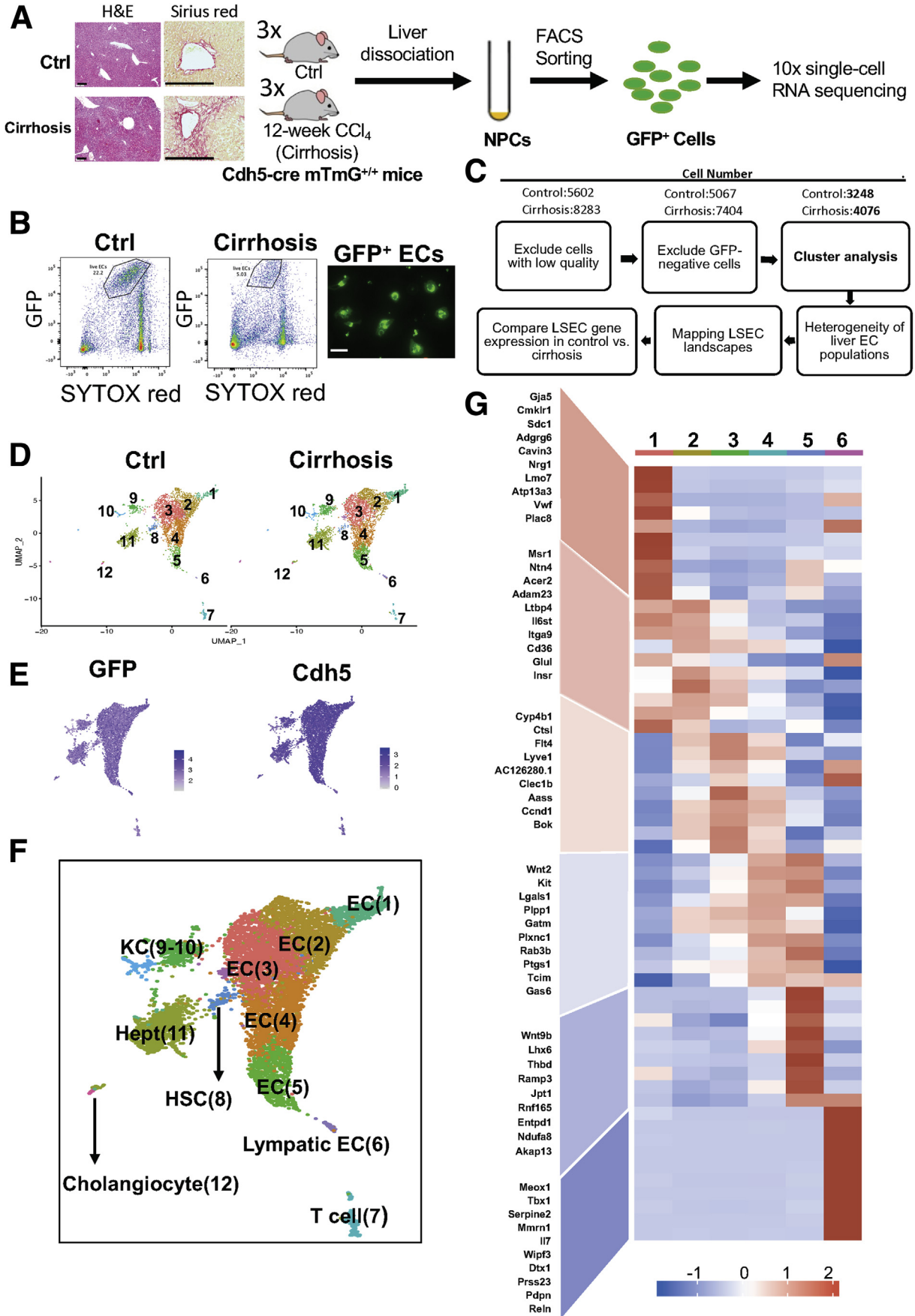
Most current article

LSEC markers in cluster 1 through 5. We found expression of a vascular EC marker, von Willebrand factor, was much higher in clusters 1 and 5 than clusters 2, 3, and 4 (Figure 3A). In contrast, an LSEC marker, Lyve1 was expressed at a higher level in clusters 2, 3, and 4 than clusters 1 and 5 (Figure 3A). In addition, these 3 clusters expressed other LSEC markers, such as Cd32b, Flt4, and Stab2, at much higher levels than clusters 1 and 5 (Figure 3A). Cd31 (Pecam1) has been reported to be more highly expressed in vascular ECs than LSECs and has been used as a marker of capillarization.[11,12] However, our data showed that all liver ECs expressed Cd31 with a slightly higher expression in clusters 1 and 5 than clusters 2, 3, and 4 (Figure 3A). Collectively, these results indicate that clusters 1 and 5 likely represent vascular EC populations, while clusters 2, 3, and 4 correspond to LSEC populations.

It was reported that Rspo3, Wnt9b, and Wnt2 were enriched in central venous ECs.[8,9] A recent paired-cell sequencing study showed these genes to be pericentral landmarks of liver ECs.[1] In our study, Rspo3 and Wnt9b were specifically expressed in cluster 5, while Wnt2 expression increased gradually from clusters 2 to 5, with the highest expression in cluster 5 (Figure 3B). In addition, we found that other pericentral landmarks, such as Kit, Cdh13, Thbd, and Fabp4,[1] exhibited expression patterns similar to that of Wnt2 (Figure 4A). Based on these observations, we consider clusters 4 and 5 to be a pericentral LSEC population (ie, zone 3 LSECs) and a central venous EC population, respectively.

We then examined expression patterns of periportal landmarks, such as Dll4 and Efnb2.[1] They were also reported to be highly expressed in arterial ECs.[7,13] Our analysis showed expression of Dll4 and Efnb2 were both the highest in cluster 1 with gradual decreases toward cluster 5 (Figure 3C). Other periportal landmarks, such as Msr1, Ltbp4, Ntn4, and Adam23,[1] also showed similar patterns to Dll4 and Efnb2 (Figure 4B). These results led us to define cluster 1 as an arterial-like EC (or portal EC) population and cluster 2 as a periportal LSEC population (ie, zone 1 LSECs). Accordingly, cluster 3 was thought to consist of midzonal (zone 2) LSECs, characterized by the highest expression of mid-zonal landmarks, Lyve1 and Ctsl (Figure 3A and D).[1,14] These results indicated that ECs of cluster 1–5 aligned from the portal tract to the central venous regions as shown in Figure 3E.

We chose 1 of the top 10 representative genes from each cluster shown in Figure 1G based on the availability of antibodies and validated their spatial distributions by immunolabeling (Figure 5A). These representative genes (proteins) are well aligned with our scRNA-seq results: von Willebrand factor for arterial-like EC (cluster 1), CD36 for periportal LSECs (cluster 2), Lyve1 for mid-zonal LSECs (cluster 3), Kit for pericentral LSECs, Thbd for central venous ECs, and IL7 for LyECs (cluster 6). Additional novel genes identified that may represent each cluster are presented in Figure 5B.

We also examined functional differences between periportal (zone 1) and pericentral (zone 3) LSECs using gene set enrichment analysis (GSEA) and identified distinct signaling pathways in zone 1 and zone 3 LSECs (Figure 4C). Given that zonal changes are gradual, we expected that LSECs of zones 1 and 3 might reveal clearer differences in pathways than those of zones 1 and 2 or zones 2 and 3.

Cluster 6: LyECs. Cluster 6 was identified as LyECs based on the expression of 4 well-known LyEC markers, Lyve1, Flt4, Pdpn, and Prox1 (Figure 6A). It is known that LSECs also express Lyve1 and Flt4, which were more highly expressed in zone 2 LSECs than in LSECs of any other zones in our analysis (Figure 3A). Therefore, we specifically compared expression levels of these 4 LyEC markers between zone 2 LSECs and LyECs (Figure 6B). Lyve1 expression was higher in LyECs than in zone 2 LSECs, while Flt4 expression was similar between these 2 groups of ECs. Pdpn and Prox1 were specifically expressed in LyECs. We also identified additional genes that were highly expressed in LyECs, but not in LSECs, including Mmrn1, Rassf9, Tbx1, and Ahnak2 (Figure 6C), and confirmed their expression by quantitative polymerase chain reaction (qPCR) using primary human LSECs and LyECs (Figure 6D).

EC Subtypes in the Entire Liver EC Population in Control vs Cirrhotic Mice

LSECs accounted for the major portion of the entire liver EC population in both control and cirrhotic mice, with 89% and 73%, respectively (Figure 7A). However, the proportions of vascular ECs (clusters 1 and 5) increased by 2–3

Figure 1. (*See previous page*). **scRNA-seq revealed a landscape of sorted liver ECs.** (A) Cell isolation workflow using endothelial-GFP reporter mice (tamoxifen inducible, cdh5-cre mTmG$^{+/+}$ mice) subjected to carbon tetrachloride (CCl$_4$) inhalation for 12 weeks to generate liver cirrhosis. Age-matched endothelial-GFP reporter mice were used as controls. Representative hematoxylin and eosin and Sirius red staining images to show liver injury and fibrotic nodules. Scale bars: 200 μm. (B) Nonparenchymal cells isolated from endothelial-GFP reporter mice were sorted to collect viable GFP-positive cells (ie, ECs). SYTOX red staining was used to exclude dead cells (SYTOX red–positive cells, left 2 panels). Sorted cells were seeded on collagen-coated plates and cultured for 24 hours. Images were taken using a Zeiss fluorescent microscope (right panel). Scale bar: 20 μm. (C) Data analysis workflow. (D) Uniformed Manifold Approximation and Projection showing sorted cell populations in control and cirrhotic mice. The cells were divided into 12 clusters. Each dot represents a single cell. (E) GFP (left) and Cdh5 (cadherin-5) (also known as VE-cadherin; right) expression among the sorted cells. All the cells used for analyses were positive with GFP and Cdh5, indicating a high purity of liver EC populations. (F) Uniformed Manifold Approximation and Projection showing 12 identified clusters of the sorted cells. The identity of each cluster was determined by matching expression profiles of clusters with established cell-specific marker genes of different hepatic cells, including ECs, LyECs, HSCs, Kupffer cells (KCs), hepatocytes (Hepts), and cholangiocytes. Numbers in parentheses indicate corresponding clusters. (H) Heatmap showing representative genes expressed by each liver EC cluster or population. These genes were determined by their average expression levels.
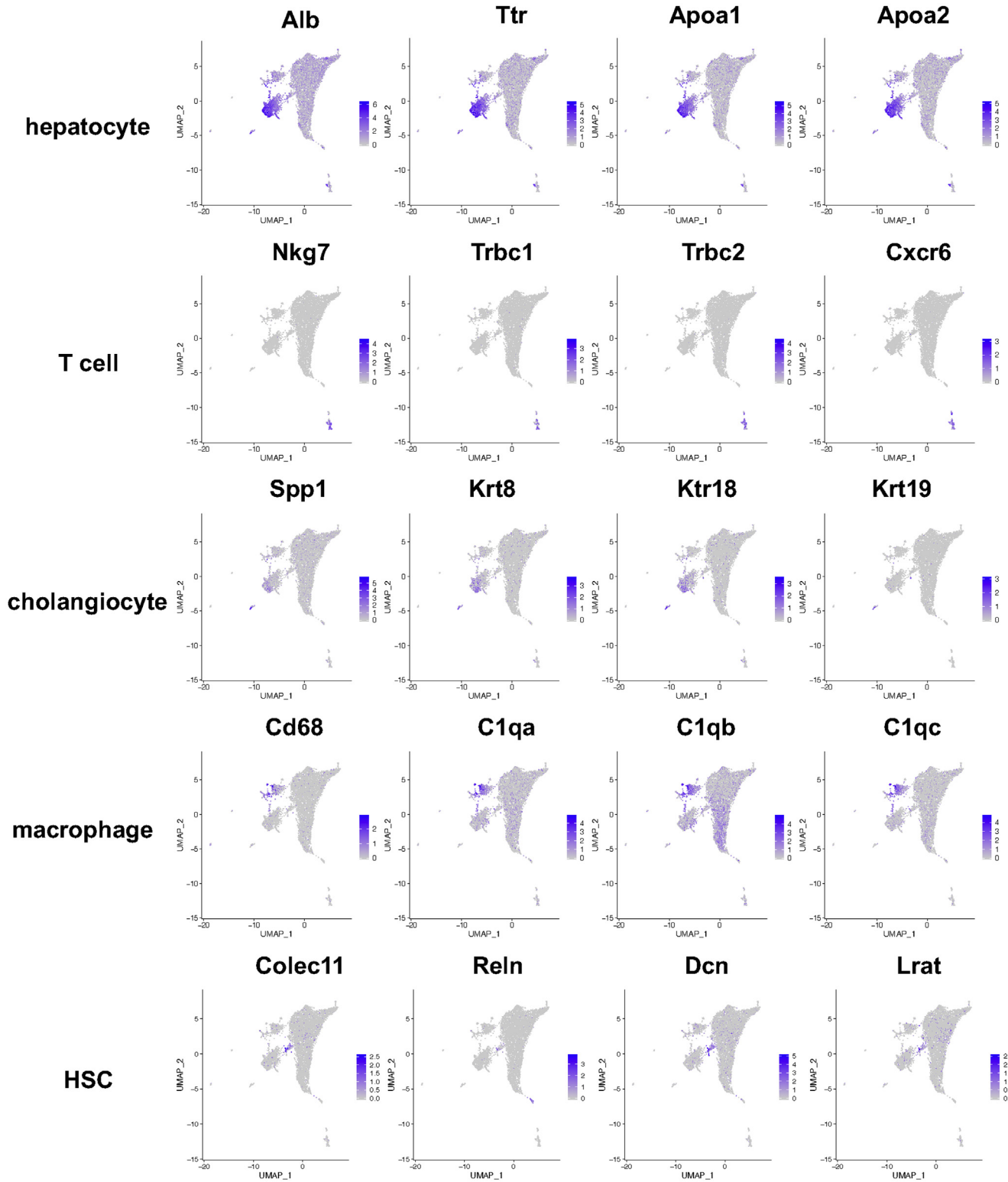
Figure 2. Clusters that expressed nonendothelial cell markers. Feature plots showing relative distributions of established marker genes of different liver cell types among the sorted cells.
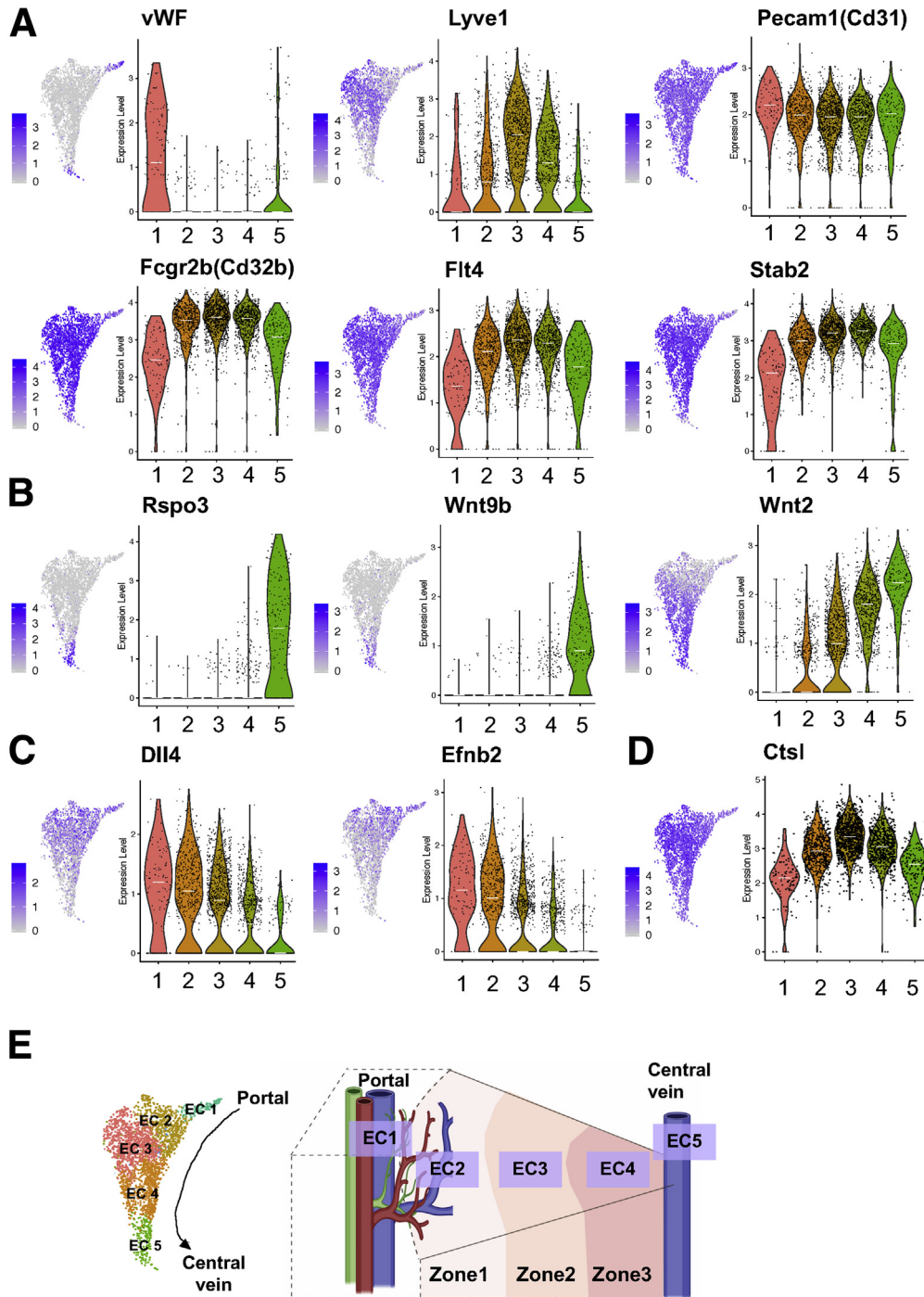
Figure 3. Spatial distributions of the identified liver EC populations (clusters 1–5) in control mice. (*A–D*) Paired feature plots (left) and violin plots (right) showing expression levels of (*A*) vascular EC and LSEC marker genes, (*B*) pericentral landmark genes, (*C*) periportal landmark genes, and (*D*) midzonal landmark genes among liver ECs 1–5. Each dot represents a single cell. In the violin plots, white lines indicate median expression values. (*E*) The identified liver ECs 1–5 were mapped on the liver lobule based on expression levels of the marker genes analyzed previously and were defined as arterial-like ECs (EC1), periportal (zone 1) LSECs (EC2), midzonal (zone 2) LSECs (EC3), pericentral (zone 3) LSECs (EC4), and central venous ECs (EC5).

times in cirrhotic mice, possibly related to increased angiogenesis in cirrhotic livers. LyECs represented only 0.12% of all liver ECs in control mice, but increased by 20-fold to 2.34% in cirrhotic mice, which was validated in immunofluorescence images of lymphatic vessels in cirrhotic and control livers (Figure 7*B*). Interestingly, although cirrhosis changed the proportions of these EC subtypes, zonal EC landmark genes were well conserved between control and cirrhotic livers (Figure 7*C*).

## Phenotypic and Functional Changes of LSECs in Cirrhotic Livers

Since LSECs account for the majority of the entire liver EC population, we examined transcriptomic changes in LSECs in liver cirrhosis.

Capillarization Was Most Prominent in Zone 3 LSECs and Represented by CD34 Induction in Cirrhotic Livers. Capillarization of LSECs is characterized by their phenotypic changes toward common vascular ECs. LSECs
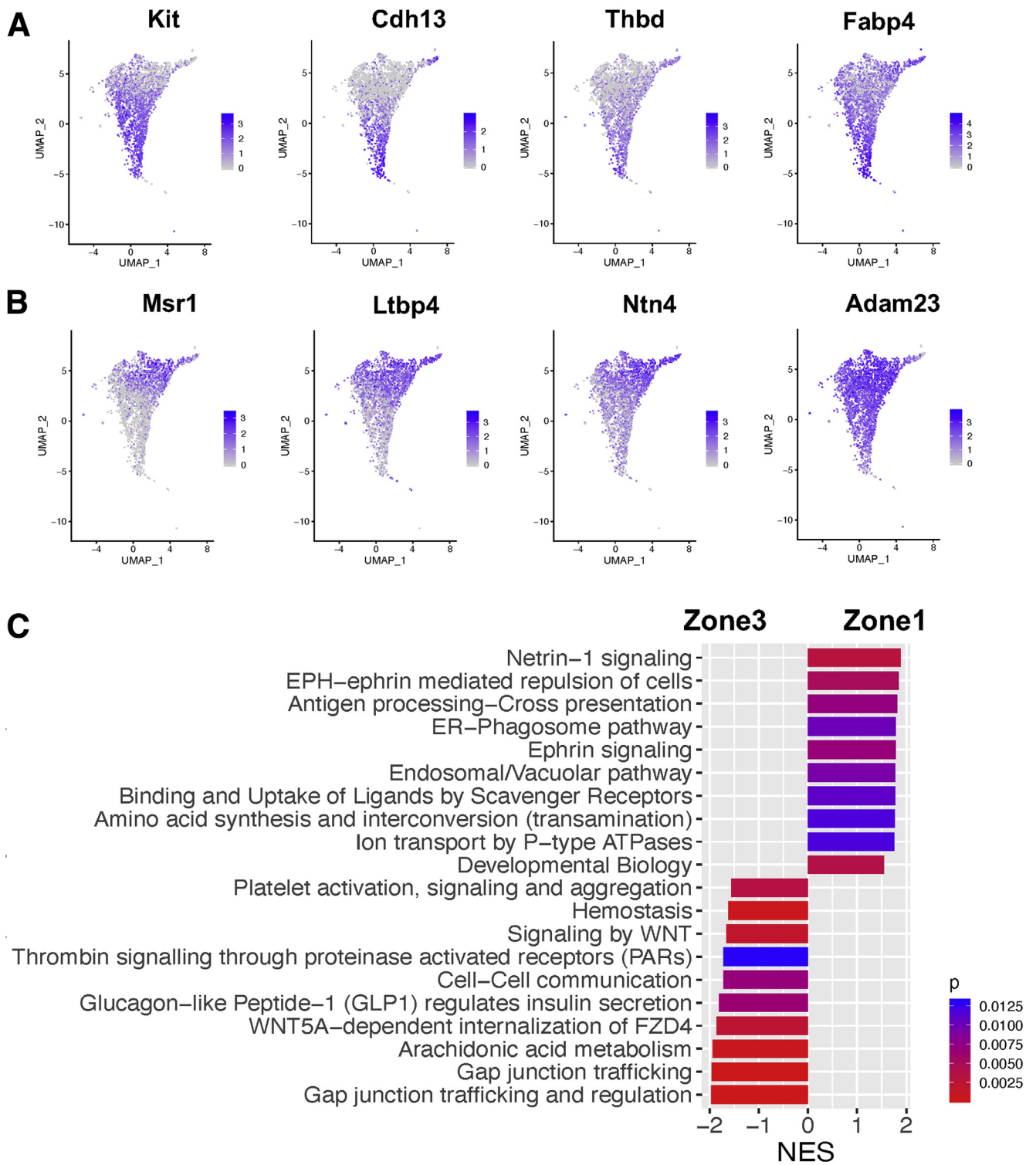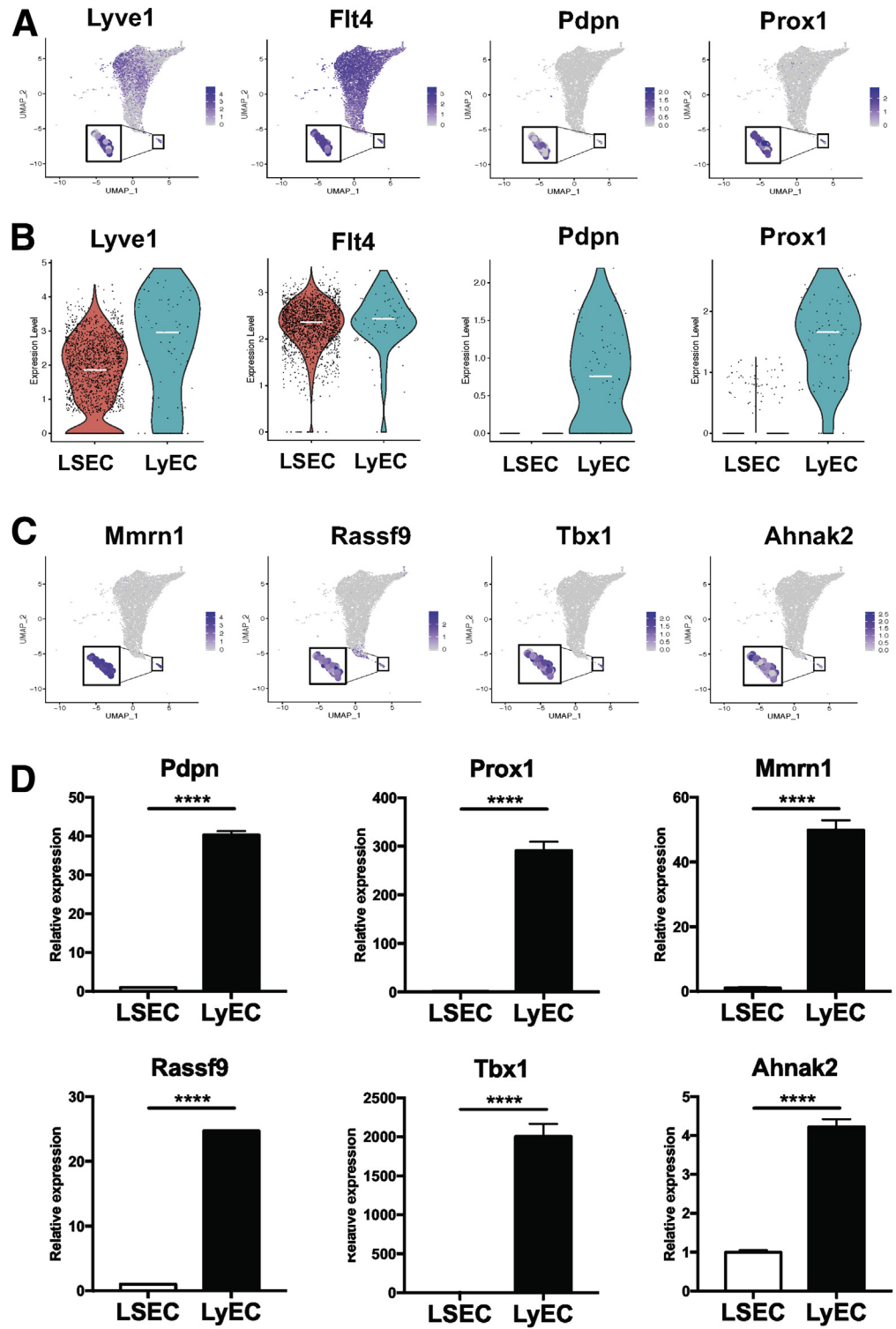
Figure 4. Relative distributions of pericentral and periportal landmark genes among all liver ECs as well as comparison of pathway analysis of periportal and pericentral LSECs. (A) Feature plots showing relative distributions of established pericentral landmark genes among all liver ECs. (B) Feature plots showing relative distributions of established periportal landmark genes among all liver ECs. (C) Comparison of signaling pathways enriched in zone 1 LSECs and zone 3 LSECs based on GSEA. The NES is the normalized enrichment score, which indicates the magnitude of the correlation of a gene set (signaling pathway) with the phenotype. A positive NES means upregulation in zone 1 LSECs relative to zone 3 LSECs, while a negative NES shows upregulation in zone 3 LSECs relative to zone 1 LSECs. The color represents a P value, which estimates statistical significance of the NES.
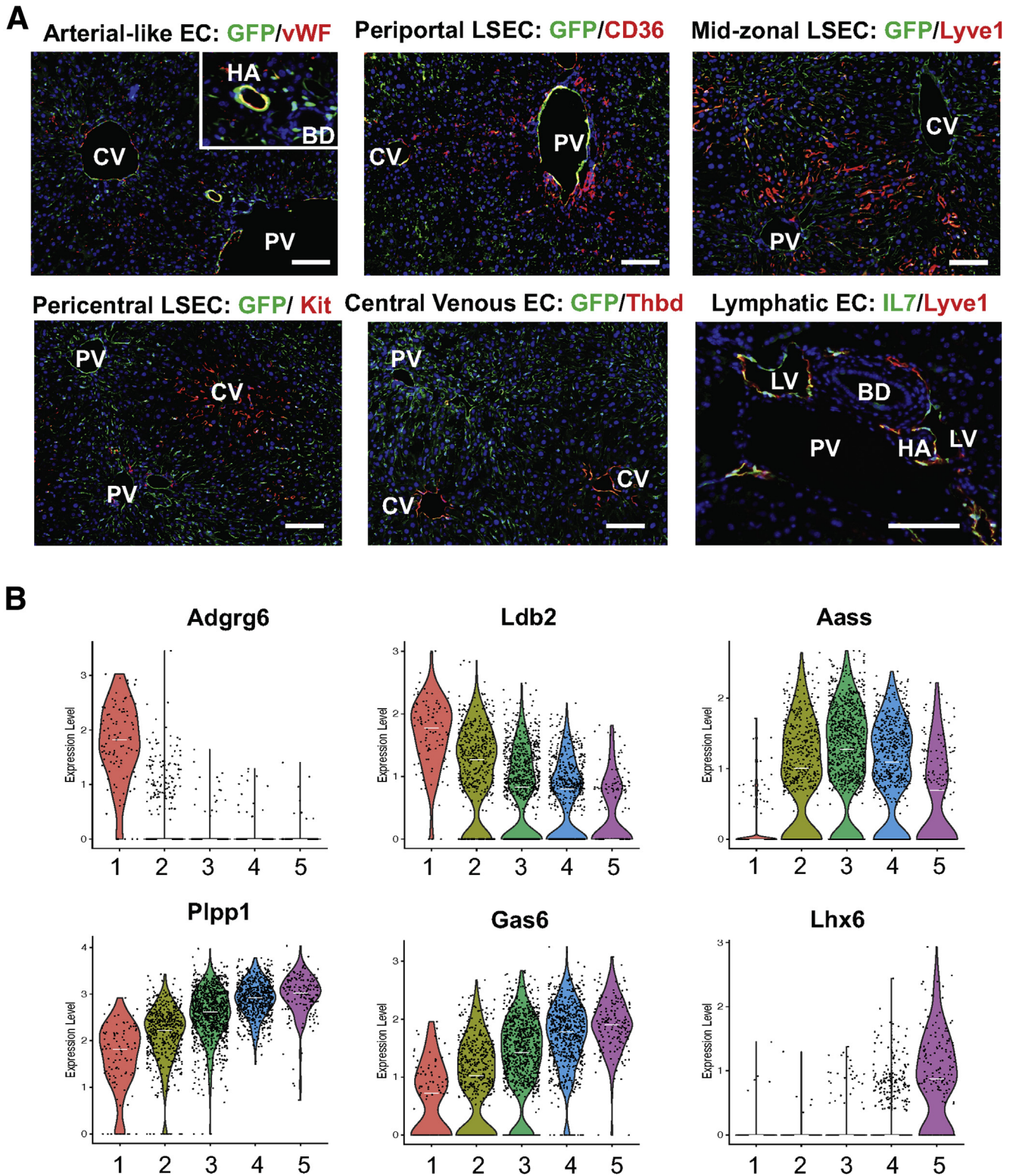
Figure 5. Validation of landmark genes by immunolabeling and expression of new liver EC landmark genes in control mice. (*A*) Immunolabeling of zone-associated landmark genes in frozen liver sections from endothelial-GFP reporter mice. Red indicates landmark genes, green indicates GFP (ECs or IL7 for LyECs), blue indicates DAPI (nuclei). Scale bar: 40 μm. Images were taken using a Zeiss fluorescence microscope. (*B*) Violin plots showing expression levels of new zone-associated landmark genes in liver ECs 1-5. Each dot represents a single cell. White lines indicate median expression values. BD, bile duct; CV, central vein; HA, hepatic artery; PV, portal vein.

Figure 6. Cluster 6 represents LyEC. (*A*) Feature plots showing relative distributions of established LyEC marker genes (Lyve1, Flt4, Pdpn, and Prox1) among all the liver ECs. Expression levels of these LyEC marker genes identified cluster 6 as LyECs. (*B*) Comparison of LyEC maker gene expression between zone 2 LSECs and LyECs. Zone 2 LSECs were chosen for the comparison because of the highest levels of Lyve1 and Flt4 that they expressed among 3 LSEC populations. Each dot represents a single cell. White lines indicate median expression values. (*C*) Feature plots showing some of the genes found only in cluster 6, which thus have the potential as new LyEC markers and could help to distinguish LyECs from LSECs. (*D*) qPCR analysis to validate unique LyEC markers (distinct from LSECs) identified in this scRNA-seq analysis. Human primary LSECs and LyECs were used for qPCR analysis. n = 3. ****$P < .0001$. qPCR analysis was repeated 3 times to confirm this finding.

have fenestrae of approximately 0.1 μm organized into groups of sieve plates, which facilitate the transport of macromolecules from hepatic sinusoids to the space of Disse. In addition, LSECs lack basement membranes, which also allows efficient transport of macromolecules between hepatic sinusoids and the space of Disse.[15] Capillarization

entails loss of fenestrae and development of basement membranes,[16,17] thus having a significant negative impact on liver homeostasis. Capillarization is also known to cause activation of HSCs and thereby liver fibrosis and cirrhosis progression.[18] Comparison of gene expression associated with LSEC capillarization between control and cirrhotic
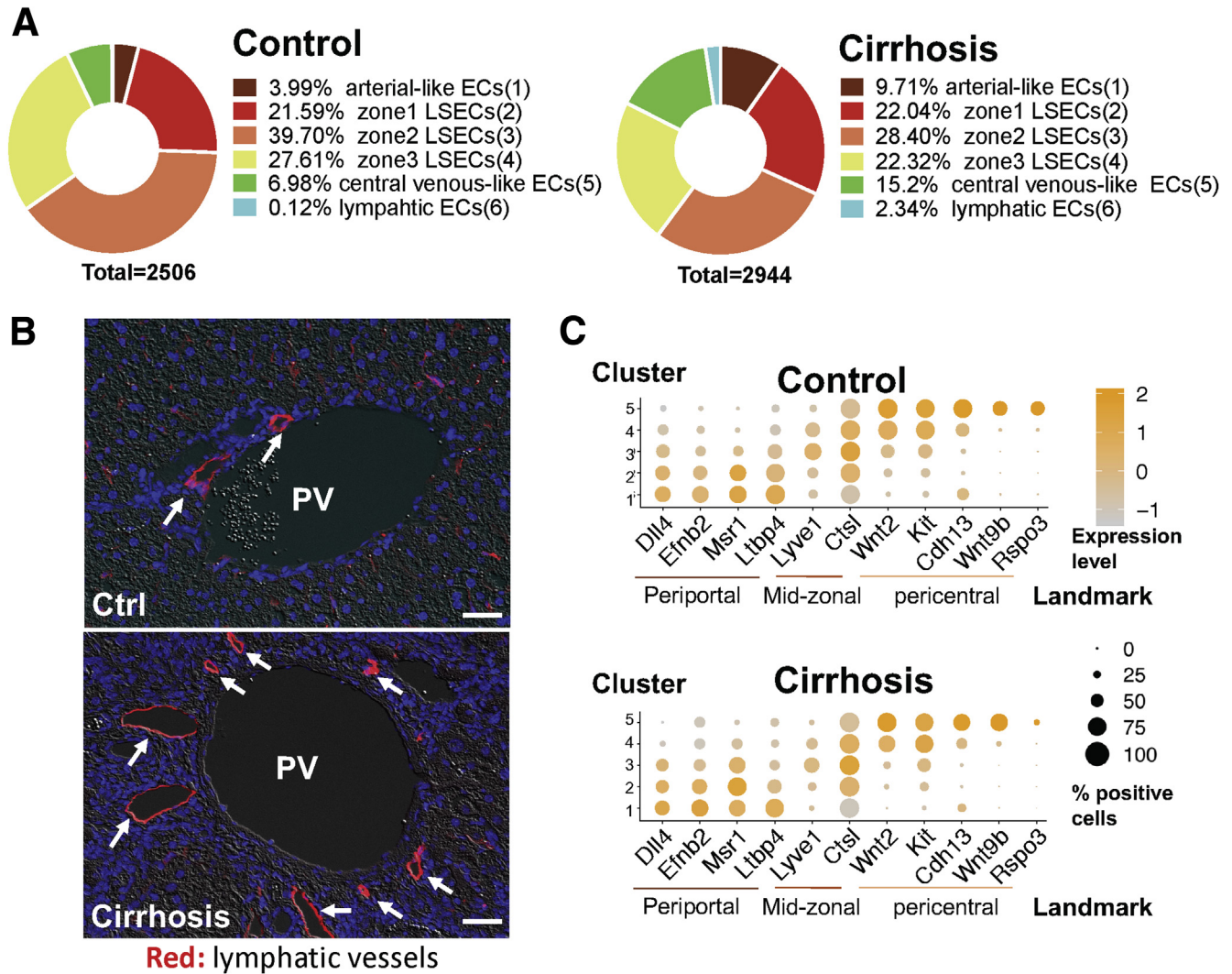
Figure 7. Liver cirrhosis alters proportions of liver EC populations but still conserves their identities. (*A*) Proportions of liver EC populations in control vs cirrhotic mice. (*B*) Immunofluorescence images of lymphatic vessels (arrows) in control and cirrhotic mouse livers. Red indicates Lyve1 (arrows indicates lymphatic vessels), blue indicates DAPI (nuclei). Because it has been known that a majority of lymphatic vessels are found in the portal tract area, Lyve1 can still b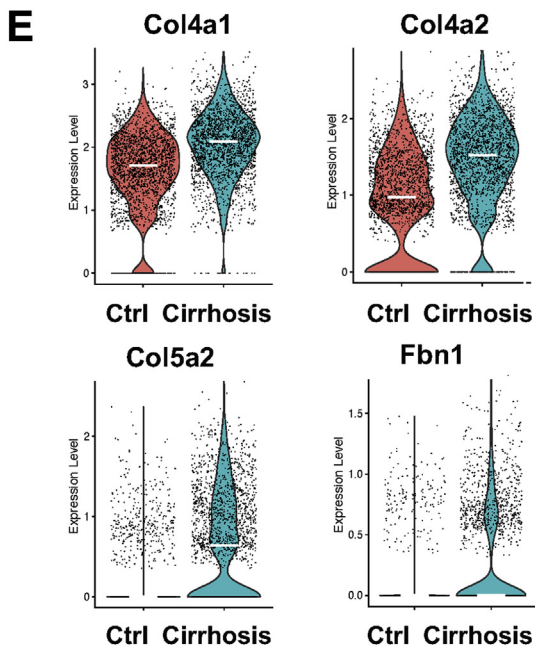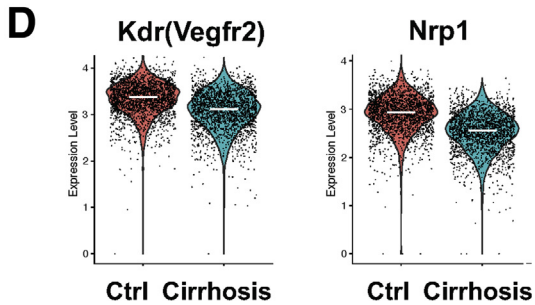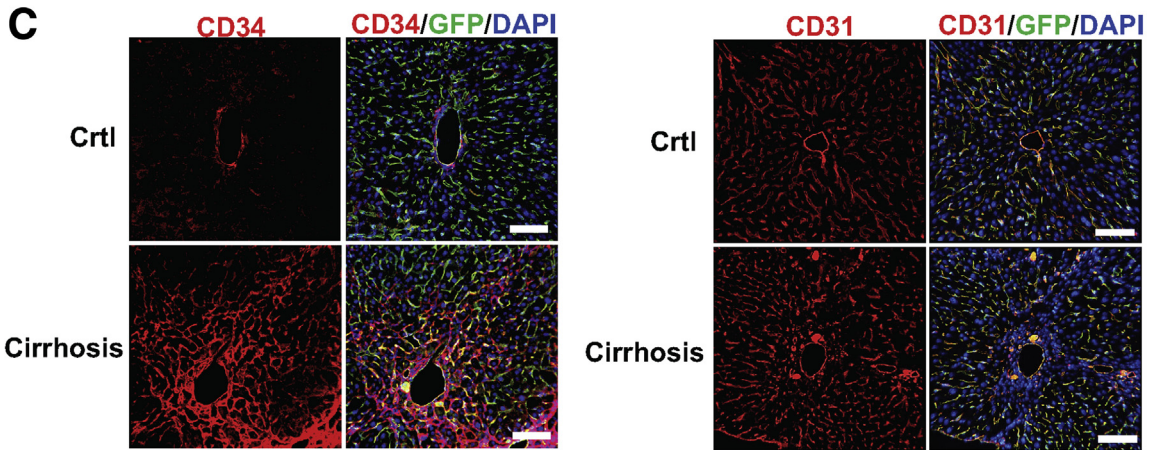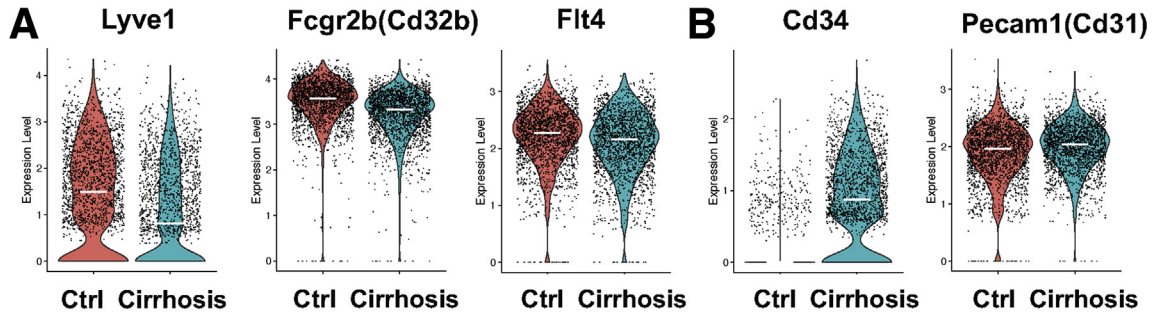e used as a lymphatic vessel marker. Scale bar: 40 μm. Images were taken using a Zeiss fluorescence microscope. (*C*) Dot plots showing conserved landmarks of liver ECs in control and cirrhotic mice. The y-axis indicates EC populations corresponding to clusters 1–5 and the x-axis refers to EC landmarks, including periportal, midzonal, and pericentral landmarks. The size of each dot represents a percentage of cells that positively express the landmark gene. Orange color indicates higher expression levels, while gray color depicts lower expression levels. PV, portal vein.

livers revealed downregulation of LSEC markers such as Lyve1, Cd32b, and Flt4 in cirrhotic mice (Figure 8A). Many studies have used upregulation of CD34 or CD31 in LSECs as a sign of LSEC capillarization,[11,12,19] while increased expression of CD31 by cirrhotic LSECs has been controversial.[10,20,21] CD31 is expressed in EC intercellular junctions. CD34 is a glycosylated transmembrane protein and is frequently regarded as a marker of hematopoietic stem cells and hematopoietic progenitor cells. However, its expression has also been recognized in a wide range of non-hematopoietic cell types, including subsets of ECs such as vascular ECs.[22] LSECs do not express CD34 in normal conditions, but do express it in pathological conditions. Its

expression is often associated with the presence of matrix proteins such as laminin, a basement membrane component.[23,24] Because the development of basement membranes is a characteristic of capillarized LSECs, CD34 has been used as a marker of LSEC capillarization. We found significant upregulation of CD34 in all zones of LSECs of cirrhotic mice (average fold change = 6.3) (Figures 8B and F), which was consistent with immunolabeling results in Figure 8C (left panels), showing prominent expression of CD34 around zone 3 in cirrhotic livers. In contrast, CD31 was highly expressed in LSECs regardless of the presence of cirrhosis with only a slight upregulation in cirrhotic livers (average fold change = 1.1) (Figure 8B), which was also

A Lyve1   Fcgr2b(Cd32b)   Flt4

B Cd34   Pecam1(Cd31)

C CD34   CD34/GFP/DAPI   CD31   CD31/GFP/DAPI

D Kdr(Vegfr2)   Nrp1

E Col4a1   Col4a2   Col5a2   Fbn1

F Cirrhosis relative to Ctrl

	Zone1	Zone2	Zone3
Lyve1	0.60	0.71	0.51
Cd32b	0.78	0.83	0.69
Flt4	-	-	0.64
Cd34	4.92	6.39	8.83
Kdr	0.90	0.83	0.64
Nrp1	0.70	0.68	0.63
Col4a1	1.45	1.49	1.71
Col4a2	1.72	1.84	2.14
Col5a2	2.72	4.21	4.12
Fbn1	1.95	3.05	3.11

down   up
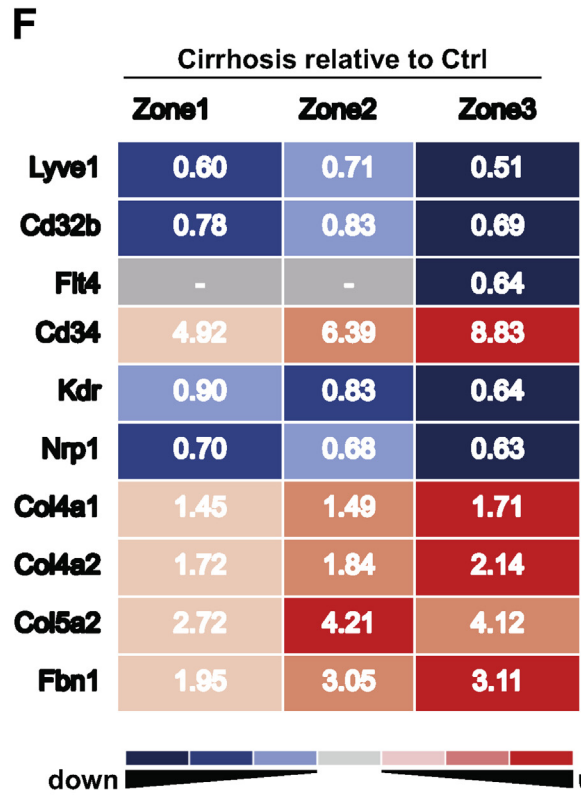
verified by immunolabeling results (Figure 8C, right panels). These results indicate that CD34 is a more accurate marker of LSEC capillarization than CD31.

Previous studies also reported that VEGF released by hepatocytes and HSCs maintained LSEC phenotype in a paracrine manner.[25] We found a VEGF receptor, Kdr (Vegfr2), and its co-receptor Nrp1 were both downregulated in LSECs of cirrhotic mice (Figure 8D), which may also explain decreased VEGF signaling and subsequent dysregulation of LSEC phenotype in cirrhotic livers. In addition, we found that extracellular matrix genes, such as Col4a1, Col4a2, Col5a2, and Fbn1, were all upregulated in LSECs of cirrhotic mice (Figure 8E), which may be related to the development of basement membranes and extracellular matrix deposition in liver fibrosis and cirrhosis. Comparison of zonal expression of the previously mentioned capillarization-associated genes between control and cirrhotic mice revealed that all these genes except for Col5a2 were most downregulated or upregulated in zone 3 LSECs (Figure 8F), suggesting that zone 3 LSECs are the most susceptible to capillarization in liver cirrhosis.

Decreased Expression of Endocytic Receptors. LSECs are involved in removal of circulating antigens and toxins through their strong endocytic capacity.[26] We found that expression of major endocytic receptors including mannose receptor (Mrc1) and scavenger receptors (Stab1, Stab2, Scarb1, and Scarb2), as well as lysosomal transport protein (Lamp2 [lysosome-associated membrane glycoprotein-2]),[27] were significantly decreased in LSECs of cirrhotic mice (Figure 9A). Interestingly, all these genes were also most downregulated in zone 3 LSECs of cirrhotic mice (Figure 9B).

Regulation of Vascular Tone. LSECs respond to increased shear stress to maintain normal vascular tone by promoting nitric oxide (NO) production by endothelial NO synthase (eNOS).[28] The loss of this property is one of the representative features of endothelial dysfunction and is observed in cirrhosis.[26,29] Some transcription factors, such as the Kruppel-like family (Klf2 and Klf4) and AP1 (activating protein-1), are induced by shear stress and are responsible for increased eNOS expression and activity.[30–32] We found downregulation of both Klf2 and Klf4 in LSECs of cirrhotic mice (Figure 10A). Similarly, some of the major AP1 components, such as Fos, Fosb, Jun, and Junb, were remarkably suppressed in LSECs of cirrhotic livers (Figure 10B).

One of the key signaling pathways regulating sinusoidal vascular tone is the endothelin signaling pathway. Endothelin receptor type A and B are encoded by Ednra and Ednrb genes, respectively.[33] In our analysis, Ednra was not expressed in LSECs either in control or cirrhotic livers (Figure 10C, upper 2 panels) as it is known to be expressed in smooth muscle cells, not in ECs,[33] while Ednrb was significantly upregulated in LSECs of all zones in cirrhotic livers (Figure 10C, lower 2 panels). In control livers, Ednrb was highly expressed only in portal ECs and some adjacent LSECs. Immunolabeling of Ednrb in control and cirrhotic livers was consistent with scRNA-seq results (Figure 10D).

Endothelial-to-Mesenchymal Transition. Several studies reported that LSECs underwent EndMT in response to chronic liver injury.[34–36] In contrast, we did not find notable increases in mesenchymal markers, such as α-smooth muscle actin (α-SMA), Sm22, Fn1, and Fsp1, in LSECs of cirrhotic mice compared with those of control mice (Figure 11A). In addition, with the exception of vimentin, other EndMT-associated genes, such as Snail1/2, Twist1, Zeb1/2, Col1a1/2, Tgfb2/3, Tgfbr3, and Tgfbi, were not upregulated in LSECs of cirrhotic mice either (Figure 11B). The absence of EndMT in LSECs of cirrhotic mice was also demonstrated by immunolabeling of α-SMA in livers from EC-GFP reporter mice subjected to CCl$_4$ inhalation for 12 weeks to induce liver cirrhosis (Figure 11C) or bile duct ligation (BDL) to induce liver injury (1-week BDL), fibrosis (2-week BDL), and cirrhosis (4-week BDL) (Figure 11D). GFP-positive cells representing all liver ECs did not colocalize with α-SMA in LSECs in either CCl$_4$ or BDL models (Figures 11C and D). However, it was noted that in an *in vitro* cell culture condition, rat primary LSECs underwent EndMT in a time dependent manner (Figure 12). Collectively, these results suggest that mouse LSECs seem resistant to EndMT in liver cirrhosis in vivo.

Pathway Analysis. To examine what biological signaling pathways are potentially altered in whole LSECs or specific zonal LSECs of cirrhotic mice, we performed GSEA. Pathways activated or suppressed in LSECs of cirrhotic mice compared with control mice are presented in Figure 13. LSECs in zones 1, 2, and 3 showed some similarities, but also showed distinct differences in signaling pathways affected by liver cirrhosis, suggesting zonal specificities of LSEC function. LSECs of all 3 zones of cirrhotic mice showed upregulation of ribosome, and PPAR signaling pathway as well as downregulation of tumor necrosis factor signaling

Figure 8. (*See previous page*). LSEC capillarization is most prominent in zone 3, and CD34 represents LSEC capillarization more accurately than CD31. (*A*, *B*) Violin plots showing expression levels of capillarization-associated genes in LSECs (clusters 2, 3, and 4) of control and cirrhotic mice. Each dot represents a single cell. White lines indicate median expression values. (*C*) Immunolabeling of CD34 or CD31 in frozen liver sections from endothelial-GFP reporter mice. Red indicates CD34 or CD31 (frequently used capillarization markers), green indicates GFP (endothelial cells), blue indicates DAPI (nuclei). Scale bar: 100 μm. Images were taken using a confocal fluorescence microscope. (*D*, *E*) Expression of Kdr, Nrp1 (genes to maintain LSEC phenotype), and extracellular matrix genes in LSECs (clusters 2, 3, and 4) of control and cirrhotic mice. Each dot represents a single cell. White lines indicate median expression values. (*F*) Differential gene expression between control and cirrhotic mice in each cluster of LSECs (corresponding to zones 1, 2, or 3). The numbers in the figure indicate fold changes of expression levels (cirrhosis relative to control). The numbers greater than 1 (red) mean upregulation in LSECs of cirrhotic livers, while those less than 1 (blue) mean downregulation. The exact number is the magnitude of the fold change. All fold changes are statistically significant (*P* < .05). The hyphen (in gray cells) indicates no statistical significance between cirrhotic and control mice.
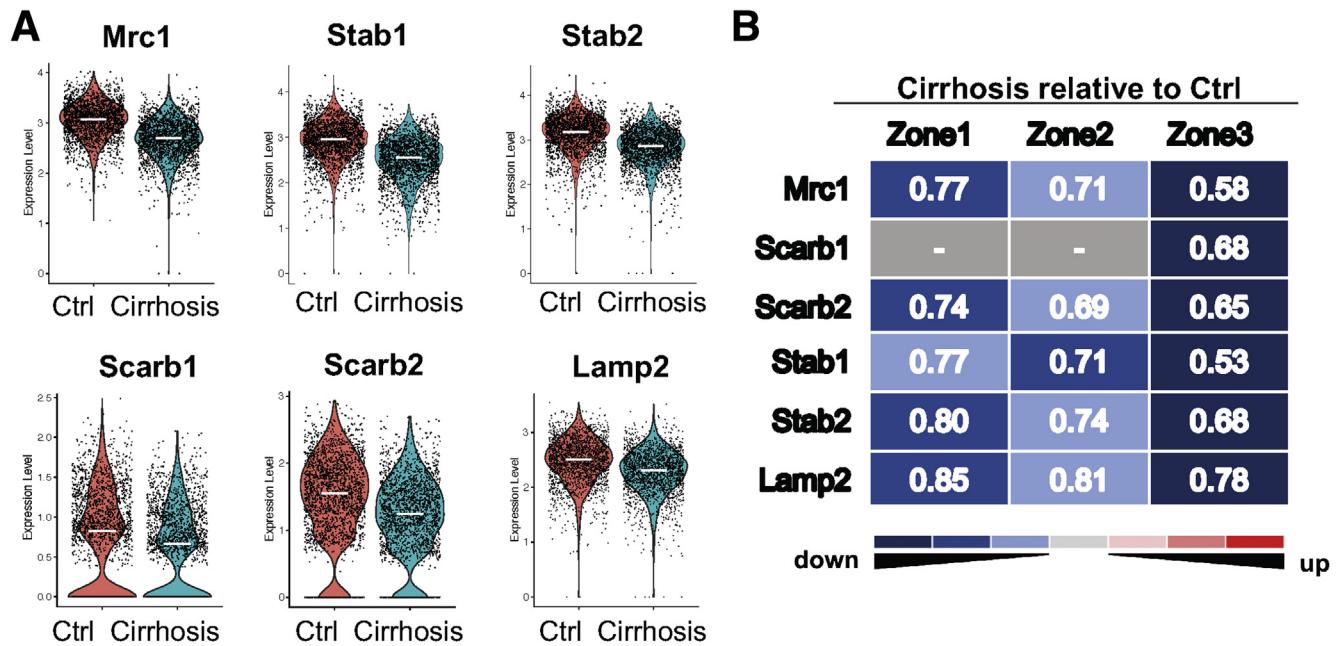
Figure 9. Cirrhosis decreases expression of endocytotic receptor genes most profoundly in zone 3 LSECs. (*A*) Violin plots showing expression levels of endocytosis receptor genes in LSECs (clusters 2, 3, and 4) of control and cirrhotic mice. Each dot represents a single cell. White lines indicate median expression values. (*B*) Differential expression of endocytosis receptor genes between control and cirrhotic mice in each cluster of LSECs (corresponding to zones 1, 2, or 3). The numbers in the figure indicate fold changes of expression levels (cirrhosis relative to control). The numbers greater than 1 (red) mean upregulation in LSECs of cirrhotic livers, while those less than 1 (blue) mean downregulation. The exact number is the magnitude of the fold change. All fold changes are statistically significant ($P < .05$). The hyphen (in gray cells) indicates no statistical significance between cirrhotic and control mice.

pathway and IL17 signaling pathway. There are some unique pathways only present or absent in specific zones. Such examples found in zone 3 LSECs include (1) the absence of upregulation of rap1 signaling, platelet activation, and actin cytoskeleton regulation pathways and (2) the presence of upregulation of gap junction signaling pathway.

Discussion

The particular importance of our study consists in spatial (ie, zonal) characterization of LSECs (zones 1–3), identification of transcriptomic changes in these zones associated with liver cirrhosis, and demonstration of relationships between these transcriptomic changes and phenotypic changes observed in liver cirrhosis. We found that zone 3 LSECs are most susceptible to damages associated with liver cirrhosis with increased capillarization and decreased abilities to regulate endocytosis. Identification of the most dysfunctional LSEC populations will be tremendously useful for the development of effective therapeutic strategies targeting them. Further, we demonstrated that CD34 is more useful as a marker of LSEC capillarization in liver cirrhosis than CD31.

The role of LSECs in the pathogenesis of liver fibrosis and cirrhosis has received a great deal of attention for many years.[18,26] Most studies have identified differentially expressed genes by quantitative real-time PCR or bulk RNA-seq using isolated primary LSECs. However, isolation of pure LSECs is challenging because LSEC preparation can easily be contaminated with other cell types, especially with vascular ECs, which may influence overall interpretation of results. Furthermore, due to heterogeneity of the LSEC population, some isolation techniques may exclude certain subpopulations of LSECs.[5,18] For example, Lyve1 is negative in some periportal LSECs, resulting in their removal when sorting is based on Lyve1 positivity.[5] One of the strengths in our study is use of EC-specific GFP reporter mice. Isolating GFP-positive cells from these mice reduced selection bias. In addition, as the isolation did not require extra marker staining, it simplified the isolation process and saved sample preparation time, helping to improve cell viability, which was especially important for fragile cells like LSECs. Furthermore, scRNA-seq analysis based on these isolated GFP-positive cells allowed us to identify highly enriched LSEC populations from all liver ECs and have all subtypes of LSECs. We think that these advantages of cell sorting conferred more reliable and comprehensive qualities to our comparison of differentially expressed genes in these identified LSECs between control and cirrhotic mice.

We found that capillarization was most severe in zone 3 LSECs, suggesting that pericentral LSECs are most vulnerable in the microenvironment of cirrhotic livers. Because blood runs from portal veins and hepatic arteries toward central veins, creating decreasing gradients of oxygen and nutrition along liver lobules with their lowest levels in the central vein areas, hepatocytes in the pericentral area may be more sensitive to anoxia and damage in cirrhotic livers.
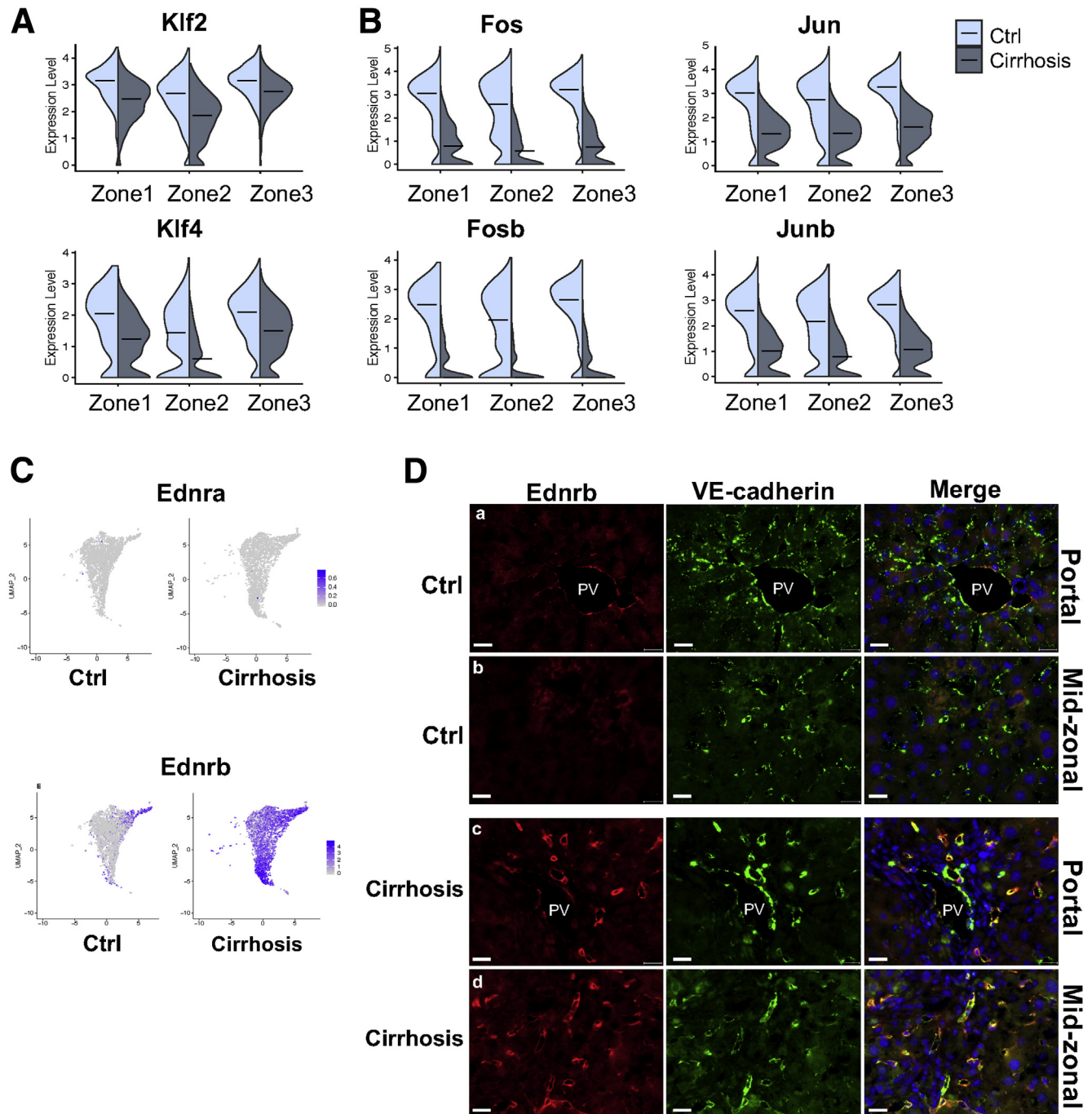
Figure 10. Identification and validation of genes associated with LSEC dysfunction in cirrhotic livers. (*A, B*) Violin plots showing expression levels of transcription factors in LSECs (clusters 2, 3, and 4) of control and cirrhotic mice. Black lines indicate median expression values. (*C*) Relative distributions of endothelin receptors (Ednra and Ednrb) in liver ECs of control and cirrhotic mice. (*D*) Immunolabeling of Ednrb in frozen liver sections from endothelial-GFP reporter mice. (*A, C*) The portal tract area and (*B, D*) the midzonal area of the liver. Red indicates Ednrb, green indicates VE-cadherin (represents all liver ECs), blue indicates DAPI (nuclei). Scale bar: 20 μm. Images were taken using a Zeiss fluorescence microscope. PV, portal vein.

An interaction of injured hepatocytes and LSECs in zone 3 may aggravate capillarization of LSECs. The mechanism of LSEC capillarization is still not well understood. It is reported that VEGF produced by hepatocytes and HSCs maintain the phenotype of LSECs.[25] However, VEGF secretion is increased in cirrhotic livers,[26] suggesting that capillarization of LSECs may be related to disruption of downstream signaling of VEGF rather than lack of VEGF. We found both VEGF receptor Kdr and co-receptor Nrp1 were most downregulated in zone 3 LSECs of cirrhotic mice as well, which may contribute to LSEC capillarization to some degree.
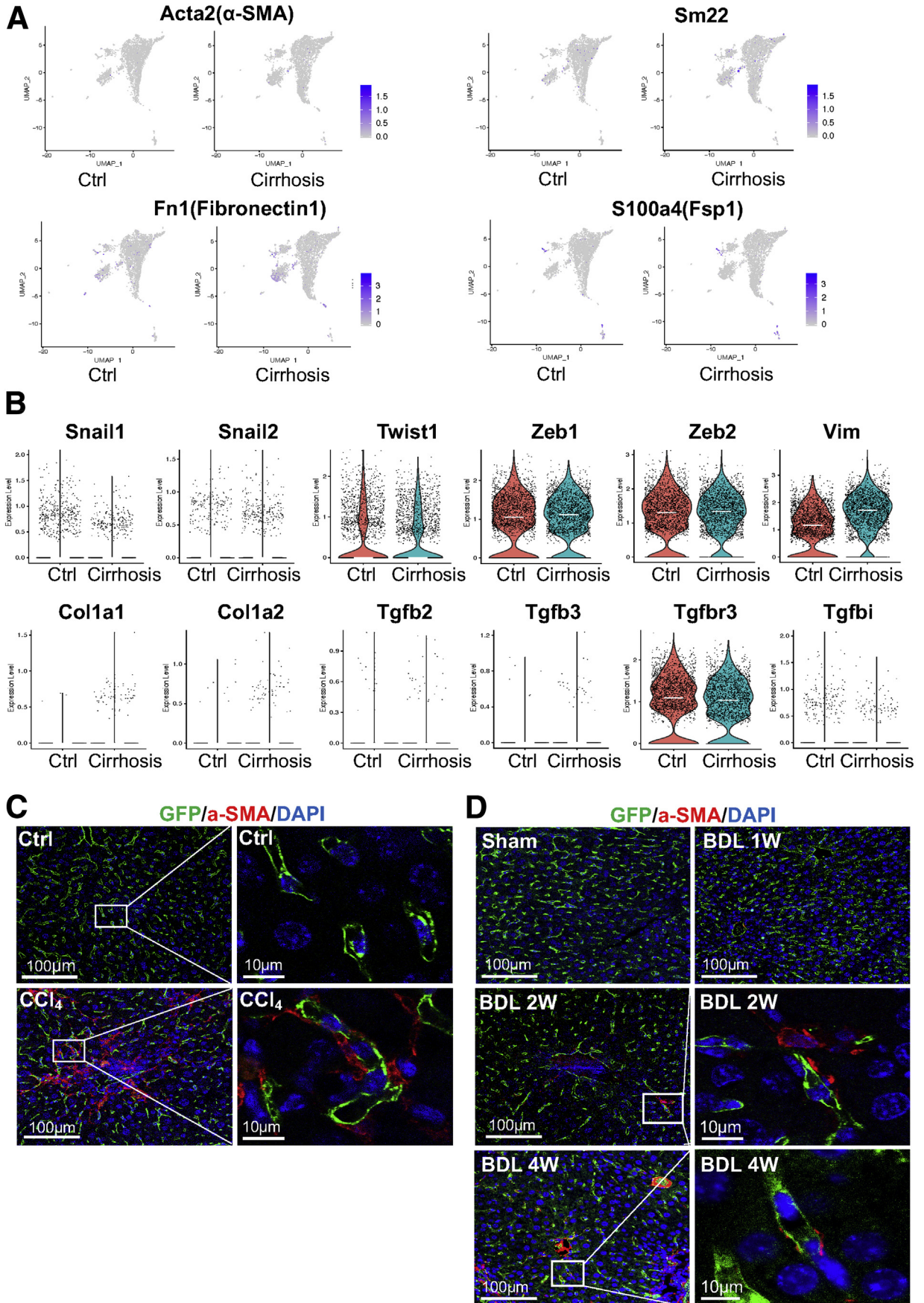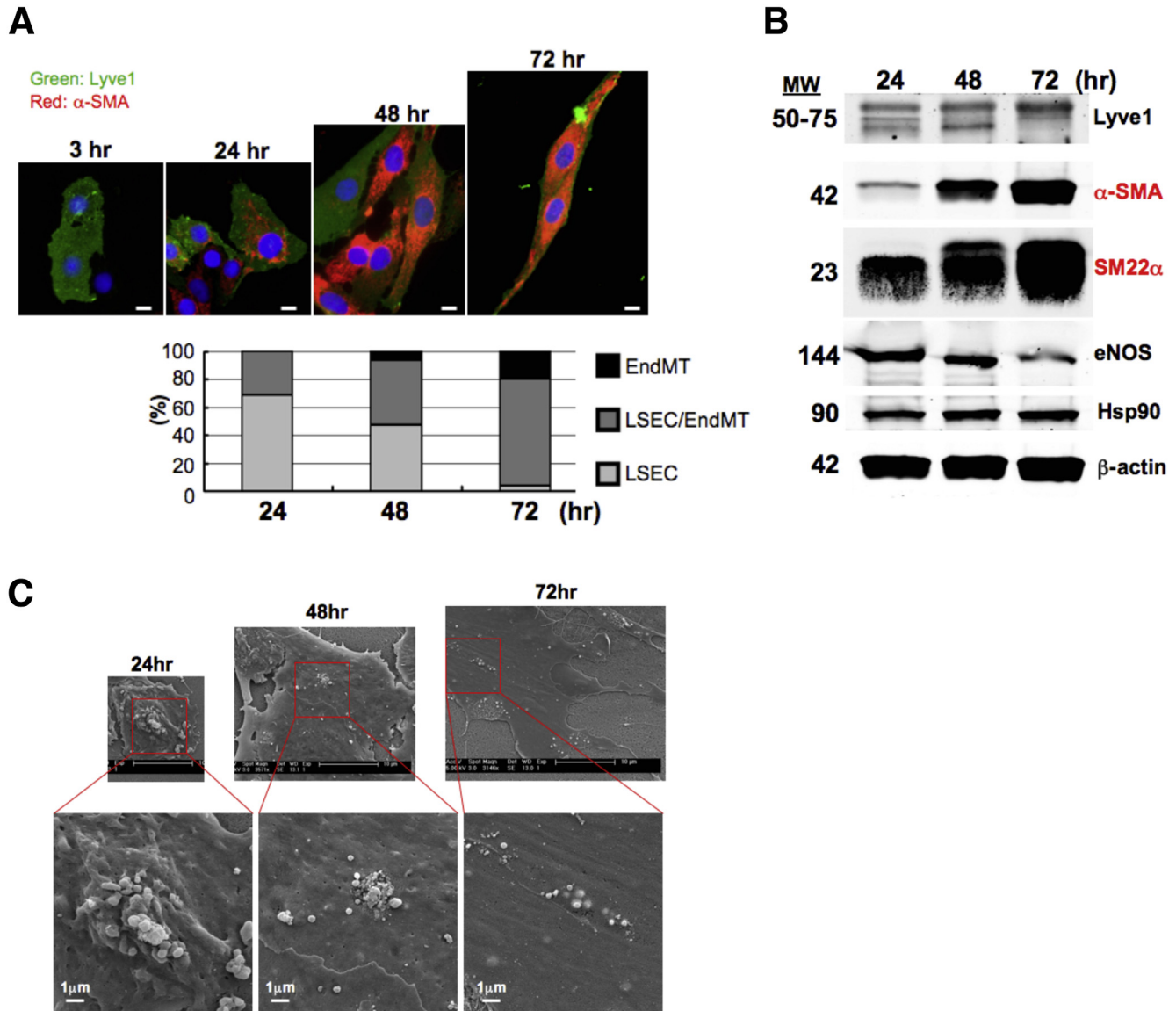
Figure 12. Rat primary LSECs undergo EndMT in a cultured condition in a time-dependent manner. (A) Immunolabeling of Lyve1 and α-SMA to assess EndMT in rat primary LSECs cultured for 3, 24, 48, and 72 hours on collagen-coated cover glasses. Green indicates Lyve1 (an LSEC marker), red indicates α-SMA (an EndMT marker), blue indicates DAPI (nuclei). Scale bar: 5 μm. (B) Western blot analysis of Lyve1 (an LSEC marker), α-SMA, and SM22α (EndMT markers) and eNOS (an EC marker). Hsp90 and β-actin were used as loading controls. (C) Scanning electron microscopy images of fenestrae in LSECs cultured for 24, 48, and 72 hours. Scale bar: 10 μm (upper panel) and 1 μm (lower panel).

LSECs are one of the most powerful scavengers in the body, playing an important role in clearance of wastes and pathogens in blood originated from the gut and the systemic circulation.[37–39] This activity is related to their expression of various endocytosis receptor genes including scavenger receptors (Scarb1, Scarb2, Stab1, and Stab2)[39] and mannose receptor (Mrc1)[40] as well as genes of related activities such as Fc gamma-receptor IIb2 (Fcgr2b/CD32b).[41] We found downregulation of all these genes in cirrhotic livers, suggesting decreased endocytic and clearance capacities of

Figure 11. (*See previous page*). **LSECs likely do not undergo EndMT in injured, fibrotic, and cirrhotic mouse livers.** (A) Relative distributions of mesenchymal marker genes in sorted cells of control and cirrhotic mice to evaluate EndMT in liver cirrhosis. (B) Violin plots showing expression levels of EndMT-associated genes in LSECs (clusters 2, 3, and 4) of control and cirrhotic mice. Each dot represents a single cell. White lines indicate median expression values. (C, D) Immunofluorescence images of paraffin liver sections (control and fibrotic or cirrhotic livers) isolated from endothelial-GFP reporter mice subjected to (C) CCl$_4$ inhalation for 12 weeks and (D) BDL. Green indicates GFP (endothelial cells), red indicates α-SMA (a mesenchymal cell marker), blue indicates DAPI (nuclei). Images were taken using a confocal fluorescence microscope.
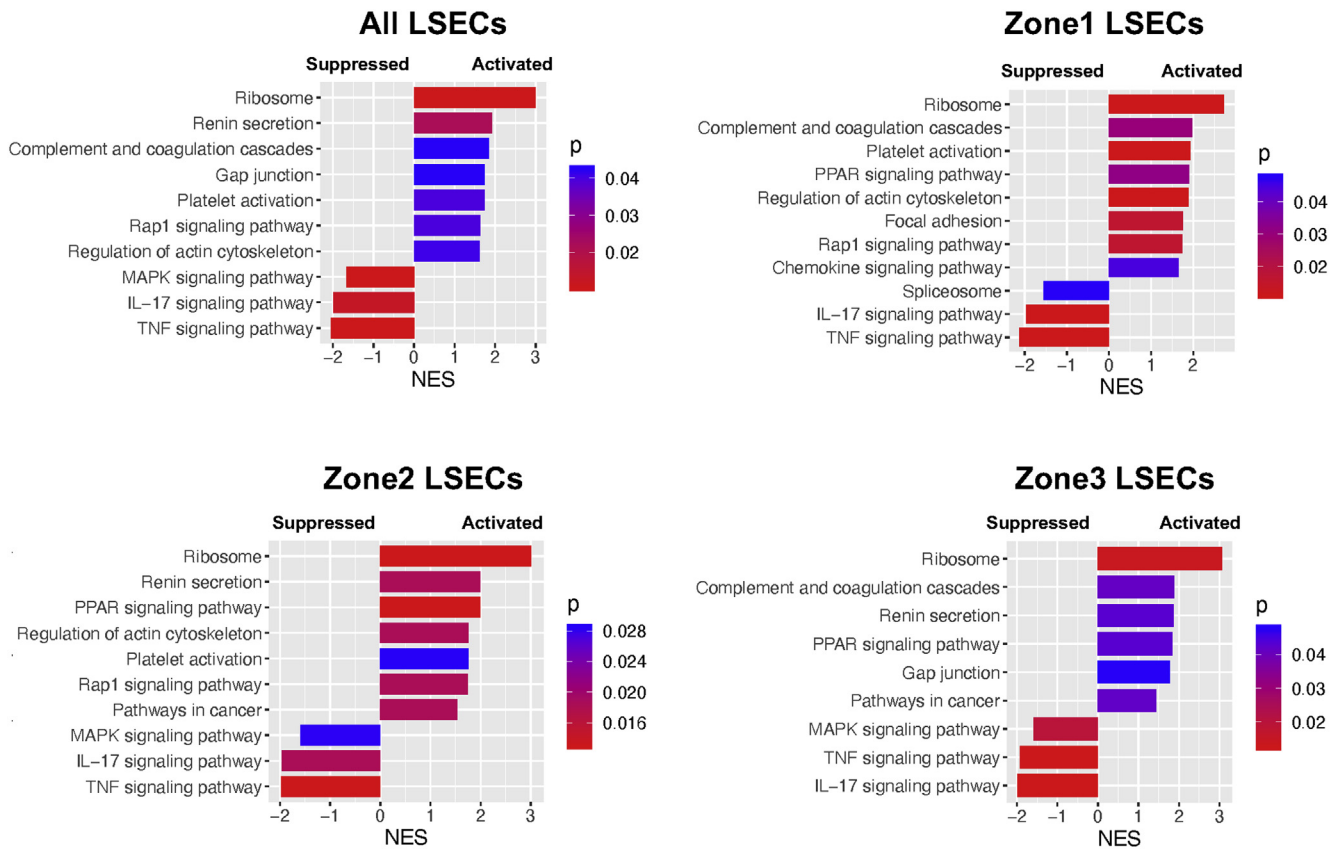
Figure 13. Pathway analysis revealed unique functional changes in zonal LSECs as a result of liver cirrhosis. Comparison of signaling pathways by GSEA based on gene expression changes in all the LSECs or within each zone of LSECs in cirrhotic mice compared with control mice. The NES is the normalized enrichment score, which indicates the magnitude of the correlation of a gene set (signaling pathway) with the phenotype. A positive NES means activation, while a negative NES shows suppression. The color represents a *P* value, which estimates statistical significance of the NES.

LSECs. This may make cirrhotic patients more susceptible to infection and systemic inflammation. Interestingly, all these endocytosis-related genes were also most downregulated in zone 3 LSECs in cirrhotic mice. The decreased endocytic capacity of LSECs may be associated with their capillarization as well, because decreased CD32b was also used as an indicator of LSEC capillarization in some studies[42]

We also found that genes known to promote eNOS expression were downregulated in LSECs of cirrhotic mice, indicating dysfunction of vascular tone observed in cirrhosis. However, our analysis also showed Ednrb expression (ET_B receptor), known to increase NO signaling in ECs,[33] was upregulated in cirrhotic livers. Ednrb upregulation was reported in human cirrhotic livers at both messenger RNA and protein levels as well.[43] Upregulation of Ednrb in LSECs could be an adaptive response to compensate for the loss of NO signaling in cirrhotic livers. Or, endothelial ET_B receptor may have different activities in physiological vs pathological conditions. One study reported that endothelial ET_B receptor contributed to vasodilatation in healthy vessels, but that endothelial ET_B-mediated vasodilation was lost in rats with pulmonary or systemic hypertension and turned into vasoconstriction.[44] In patients with cardiovascular pathologies such as atherosclerosis

and/or type 2 diabetes, ET_B-mediated vasodilation is also lost.[45,46] It was reported endothelin-1 could increase expression and activity of arginase-2[47] as well as LOX1 (oxLDL receptor-1)[48] via endothelial ET_B receptor in atherosclerotic disease. Arginase-2 can reduce NO production by competing with eNOS for a common substrate (L-arginine),[47] while oxLDL is able to impair endothelial relaxation by reducing eNOS expression and inducing reactive oxygen species.[48] Further, chronic ET_B antagonism in cirrhosis was shown to lead to less fibrosis.[49] This may suggest that overexpression of ET_B receptor by LSECs may have a profibrotic effect. Thus, it is possible that ET_B receptor in LSECs of cirrhotic livers may have other dominant downstream signaling pathways associated with endothelial dysfunction, which is an important area of future research.

EndMT refers to a process in which ECs lose endothelial markers like VE-cadherin and CD31 and gain mesenchymal markers such as α-SMA and Fsp1.[50] Several studies on fibrotic diseases, including cardiac fibrosis,[51] renal fibrosis,[52] and pulmonary fibrosis,[50] indicated that ECs could give rise to myofibroblasts through EndMT. In liver fibrosis as well, some studies indicated EndMT in LSECs.[34–36] In contrast, we did not find evidence of EndMT in LSECs in cirrhotic livers, although LSECs underwent

EndMT in a cultured condition in a time-dependent manner (Figure 12). Even if liver ECs underwent EndMT in vivo, their population would be very small, as also indicated by Ribera et al,[34] who observed EndMT only in about 4% of the liver EC population from cirrhotic livers. Our results indicate that unlike ECs in other organs, LSECs seem highly resistant to EndMT even in conditions of chronic stress and injury. Identification of the mechanism preventing LSECs from EndMT in vivo, but not in vitro, may help to develop or maintain LSECs that can be used for a variety of research and clinical purposes including generation of an engineered liver.

A recent scRNA-seq study of human-derived liver non-parenchymal cells (NPCs) from normal and cirrhotic patients identified 2 disease-specific EC populations, characterized by $CD34^+PLVAP^+VWA1^+$ and $CD34^+PLVAP^+ACKR1^+$.[6] The authors named them "scar-associated ECs" but did not demonstrate their origins. Our study did not find any disease-specific EC populations and showed similar genetic landscapes of liver ECs between control and cirrhotic mice. However, similar to the study of NPCs from cirrhotic patients, we observed significant upregulation of CD34 (Figure 8B and C), PLVAP, and ACKR1 (supplemental datasets of differentially expressed genes) in LSECs of all zones in cirrhotic livers. This result may suggest that the disease-specific EC populations found in human cirrhotic livers derive from LSECs, whose gene expression profiles are altered in liver cirrhosis. The presence of the disease-specific EC populations might also be attributable to the heterogeneity of genetic backgrounds or different stages of liver fibrosis in those human patients. Otherwise, the difference between their results and ours may come from the difference of the study subjects (ie, humans and mice). It should be mentioned that the same group of researchers recently showed the zonation pattern of HSCs, which was conserved between healthy and fibrotic mouse livers.[3] Interestingly, they also found that pericentral HSCs were predominant pathogenic collagen-producing HSCs in liver fibrosis, which may be related to our finding that zone 3 LSECs are most susceptible to capillarization.

In conclusion, the current study illustrated zonal transcriptomic alterations of LSECs in cirrhotic mouse livers and related them to phenotypic changes of LSECs observed in liver cirrhosis, which deepens our knowledge of the pathogenesis and pathophysiology of cirrhosis at a spatial, cell-specific level and helps to advance biomedical research, both basic and clinical, on liver cirrhosis. In the era of precision medicine, microenvironmental information like that presented in this study is indispensable for the development of novel and effective therapeutic strategies to target the most dysfunctional ECs and mitigate their profibrotic activities in liver fibrosis and cirrhosis.[12]

Materials and Methods
Animals

Cdh5-CreERT2, mT/mG mice were used.[53] GFP expression in ECs was induced by intraperitoneal injection of tamoxifen (Sigma-Aldrich, St Louis, MO) at a dose of 100 μg/

g body weight for 5 consecutive days. Liver fibrosis and cirrhosis was induced by inhalation of vaporized carbon tetrachloride (CCl_4) for 12 weeks[54] and BDL for 1, 2, or 4 weeks.[55] For the CCl_4 model, mice started to receive the treatment around 4 weeks of age. For the BDL model, mice at the age of around 2 months were used. Age-matched mice and sham-operated mice were used as control animals for the CCl_4 and BDL models, respectively. All animal experiments were approved by the Institutional Animal Care and Use Committees of Yale University and the Veterans Affairs Connecticut Healthcare System and were performed in accordance with the National Institutes of Health Guide for the Care and Use of Laboratory Animals.

Cell Isolation

Liver NPCs were isolated from control mice and mice subjected to CCl_4 inhalation for 12 weeks as previously described with some modifications.[56] Briefly, liver cell suspensions were obtained by collagenase (Type 2, LS004176; Worthington Biochemical Corporation, Lakewood, NJ) perfusion and were spun down at 100 g for 5 minutes to remove hepatocytes. The supernatants were pelleted at 350 g for 10 minutes and resuspended in EBM-2 (CC-3156; Lonza, Morristown, NJ). Isolated NPCs were stained with SYTOX red (5 μM; Invitrogen, Carlsbad, CA) to label dead cells and sent to FACS. Only live GFP-positive cells were sorted with BD FACSAria IIu (BD Biosciences, San Jose, CA) using a 100-μm nozzle.

10x Sample Processing and Complementary DNA Library Preparation

Samples were prepared according to the instructions of 10x Genomics Single Cell 3, Reagent Kits v3 (10x Genomics, Pleasanton, CA). Briefly, sorted cells (live GFP-positive cells) were pelleted and resuspend to attain a concentration of 1000 cells/μL. The cell number and viability were evaluated again with Trypan blue (Gibco, Waltham, MA) and a hemocytometer and confirmed with an automated cell counter. Both samples (control and CCl_4 groups) consisted of >80% viable cells. Single-cell suspensions in RT Master Mix (10x Genomics) were then loaded onto the 10x Genomics Single Cell B Chip to convert poly-adenylated messenger RNA into barcoded complementary DNA (cDNA). Barcoded cDNA was amplified by PCR to generate a sufficient mass for library construction. Enzymatic fragmentation and size selection were then used to optimize the cDNA amplicon size prior to library construction, which included end-repair, A-tailing, adaptor-ligation, and sample indexing PCR to produce Illumina-ready sequencing libraries.

Sequencing and Data Analysis

Sequencing was run on the HiSeq 4000 system (Illumina, San Diego, CA) at the Yale Center for Genome Analysis at Yale University. Each sample was sequenced across 2 lanes of the HiSeq, generating 100-bp paired-end reads at a depth of 9000 reads per cell. Preliminary standard analysis steps such as alignment and gene counting were performed based

on Cell Ranger pipelines (10x Genomics). Cell Ranger outputs were loaded into Seurat v3.0 package (http://satijalab.org/seurat/) to cluster and visualize scRNA-seq data. Genes detected in at least 3 cells were included. Cells that expressed fewer than 200 genes or had high mitochondrial genome transcript ratios (>0.2) were excluded. In order to exclude non-ECs, we filtered out cells that did not express GFP. After normalizing the data using a global-scaling normalization method "LogNormalized" and scaling the data, principal component analysis was performed to reduce the number of dimensions. Cell clusters were visualized by Uniform Manifold Approximation and Projection. Symbol gene IDs were converted to Entrez gene IDs, and GSEA was performed using the ClusterProfiler package.[57]

LSEC and LyEC Culture

Primary human LSECs and LyECs were purchased from PELOBiotech (PB-CH-153-5511; PELOBiotech, Munich, Germany) and PromoCell (C 12217; PromoCell, Heidelberg, Germany), respectively. LSECs were seeded on fibronectin-coated cell culture plates and grown in Cellovations Endothelial Cell Growth Media (PB-MH-100-4099; PELOBiotech) supplemented with 5% fetal calf serum and growth factor cocktail according to the manufacturer's instructions. LyECs were seeded on cell culture plates coated with Speed Coating Solution (PB-LU-000-0002-00, PELOBiotech) and cultured in Endothelial Cell Growth Medium MV 2 (C-22221; PromoCell) with Growth Medium MV 2 SupplementPack (C-39221; PromoCell). All cells were cultured at $37^{\circ}C$ in a humidified 5% CO_2 atmosphere.

Quantitative Real-Time PCR

Total RNA was extracted from primary human LSECs (PB-CH-153-5511; PELOBiotech) and LyECs (C-12217; PromoCell) using Trizol reagent (Invitrogen). Total RNA (1 μg) was reverse transcribed into cDNA using Reverse Transcript Reagents kit (04897030001; Roche Molecular Systems, Branchburg, NJ). qPCR was performed on cDNA with TaqMan Real-time PCR Assays (Thermo Fisher Scientific, Waltham, MA), including human 18S (Hs99999901), human Mmrn1 (Hs01113299), human Prox1 (Hs00896293), human Pdpn (Hs00366766), human Rassf9 (Hs00193763), human Tbx1 (Hs00962558), and human Ahnak2 (Hs00292832). The ABI 7500 real-time PCR system (Applied Biosystems, Foster City, CA) was used for amplification.

Immunofluorescence

Paraffin sections were de-paraffinized with xylene and rehydrated with graded ethanol. Frozen sections were washed by phosphate-buffered saline (PBS) for 10 minutes 3 times. Antigen retrieval was performed using BD solution in a steamer for 20 minutes. Blocking of nonspecific signal was performed with blocking buffer (5% donkey serum and 0.3% Triton X-100 in PBS) for 1 hour. Primary antibodies were incubated overnight at $4^{\circ}C$ (rabbit anti-α-SMA, 1:300, ab124964; rabbit anti-CD34, 1:100, ab81289; rabbit anti-Ednrb, 1:100, ab117529; rabbit anti-Lyve1, 1:300,

ab14917, [Abcam, Cambridge, MA]; rat anti-CD31, 1:100, 550274 [BD Pharmingen, San Diego, CA]; goat anti-VE-cadherin, 1:200, sc-6458 [Santa Cruz Biotechnology, Dallas, TX]; rabbit anti-vWF, 1:100, A0082 [Agilent Dako, Santa Clara, CA]; rabbit anti-CD36, 1:100, 18836-1-AP [Proteintech, Rosemont, IL]; goat anti-Thrombomodulin, 1:20, AF3894, goat anti-c-kit, 1:20, AF1356 [R&D Systems, Minneapolis, MN]). Then, secondary antibodies were incubated for 30 minutes at room temperature (donkey anti-rabbit Alexa 647, 1:300; donkey anti-rat Alexa 647, 1:300; donkey anti-goat Alexa 488, 1:300; Invitrogen). After samples were mounted with Fluoroshield containing DAPI (Sigma-Aldrich), their images were taken with a fluorescence microscope (Zeiss Observer Z1, Zeiss, Oberkochen, Germany) or confocal microscope (Leica SP5, Wetzlar, Germany).

For staining of IL7, a novel LyEC marker, IL7 promoter–driven GFP knock-in heterozygote mice were used (a kind gift from Dr. Joao Pereira, Yale University).[58] Frozen liver sections were processed with primary antibodies (rabbit anti-GFP, 1:100, 2083201; rat anti-Lyve1, 1:300, 2175430; Invitrogen) and secondary antibodies (donkey anti-rabbit Alexa 488, 1:300; donkey anti-rat Alexa 647, 1:300, Invitrogen) as described previously. Their images were taken with a fluorescence microscope (Zeiss Observer Z1).

Isolation of LSEC-Enriched Fraction From Rat Livers

Liver NPCs were isolated from Sprague Dawley rats as described previously for mouse livers.[56] Briefly, after collagenase perfusion and removal of hepatocytes, an NPC fraction was pelleted at 350 g for 10 minutes and resuspended in EBM-2 Basal Medium (CC-3156; Lonza) supplemented with Microvascular Endothelial Cell Growth Medium-2 SingleQuots supplements (CC-4147; Lonza) and 15% fetal bovine serum. The NPC suspension was subjected to a density gradient centrifugation using Percoll (GE Healthcare, Chicago, IL; Lot 10221921) at 900 g for 20 minutes at room temperature. An LSEC-enriched fraction was isolated and seeded on collagen-coated coverslips or cell culture dishes. At 3 hours, 24 hours, 48 hours, or 72 hours after cell culture in the EC medium described previously at $37^{\circ}C$ in a humidified atmosphere containing 5% CO_2, LSECs were used for immunofluorescence staining, Western blot analysis, or scanning electron microscopy.

Immunocytochemistry of LSECs

LSECs seeded on cover glasses were fixed with 4% paraformaldehyde for 20 minutes, permeabilized with 0.1% Triton X-100 for 15 minutes, blocked with 5% donkey serum for 60 minutes, and incubated with primary antibodies in a humidified chamber overnight. Rabbit anti-Lyve1 (1:100, ab14917; Abcam) and mouse anti-α-SMA (1:300, M0851; Agilent Dako) were used as the primary antibodies.

Western Blot

Proteins were extracted from LSECs using a lysis buffer containing 50 mmol/L Tris-HCl, 0.1 mmol/L EGTA, 0.1 mmol/L EDTA, 0.1% sodium dodecyl sulfate, 0.1% deoxycholic acid, 1% (vol/vol) Nonidet P-40, 5 mmol/L sodium fluoride, 1 mmol/L sodium pyrophosphate, 1mmol/L activated sodium vanadate, 0.32% protease inhibitor cocktail (Roche Diagnostics, Mannheim, Germany), and 0.027% Pefabloc (Roche Diagnostics). Protein concentrations were measured using a modified Lowry assay method with DC protein assay reagents (Bio-Rad Laboratories, Hercules, CA). A total of 20 μg of protein was loaded and separated by sodium dodecyl sulfate polyacrylamide gel electrophoresis. Proteins transferred to 0.2 μm nitrocellulose membranes (Bio-Rad Laboratories) were analyzed by immunoblotting with primary antibodies including rabbit anti-α-SMA (1:3000, ab124964; Abcam), rabbit anti-SM22α (1:3000, ab14106; Abcam), mouse anti-eNOS (1:1000, 610297; BD Biosciences), mouse anti-HSP90 (1:1000, 610419; BD Biosciences), and mouse anti-β-actin (1:3000, A1978; Sigma-Aldrich). After washing with Tris-buffered saline containing 0.1% Tween-20, membranes were incubated with fluorophore-conjugated secondary antibodies (LI-COR Biotechnology, Lincoln, NE) having 680-nm or 800-nm emission. Proteins were visualized and quantified using the Odyssey Infrared Imaging System (LI-COR Biotechnology). Hsp90 (heat shock protein 90) and β-actin were used as loading controls.

Scanning Electron Microscopy

LSECs were seeded on collagen-coated cover glasses in 12-well tissue culture plates. After 24 hours, 48 hours, and 72 hours, LSECs were fixed with 2.5% glutaraldehyde in 0.1M cacodylate buffer with pH 7.4 at room temperature for 30 minutes and then moved to 4°C for 1 hour. After washing with PBS, LSECs were treated with 1% tannic acid in 0.15M cacodylate buffer for 1 hour, then fixed with 1% osmium tetroxide in 0.1M cacodylate buffer for 30 minutes, dehydrated with graded alcohols, dried with hexamethyldisilazane, and examined using a scanning electron microscope (Hitachi SU-70; Hitachi, Tokyo, Japan).

Statistical Analysis

For scRNA-seq data, differential expression of genes between clusters or treatment groups were calculated using the Wilcoxon rank sum test implemented in Seurat v3.0 package. qPCR results for validation of differentially expressed genes between primary LSECs and LyECs were evaluated by Student's t test using GraphPad Prism 7 (GraphPad Software, San Diego, CA). Adjusted P values or P values $<.05$ were considered statistically significant.

Data Availability

GEO accession number (GSE147581) will be publicly available upon publication of this manuscript.

References

1. Halpern KB, Shenhav R, Massalha H, Toth B, Egozi A, Massasa EE, Medgalia C, David E, Giladi A, Moor AE, Porat Z, Amit I, Itzkovitz S. Paired-cell sequencing enables spatial gene expression mapping of liver endothelial cells. Nat Biotechnol 2018;36:962–970.

2. Halpern KB, Shenhav R, Matcovitch-Natan O, Toth B, Lemze D, Golan M, Massasa EE, Baydatch S, Landen S, Moor AE, Brandis A, Giladi A, Avihail AS, David E, Amit I, Itzkovitz S. Single-cell spatial reconstruction reveals global division of labour in the mammalian liver. Nature 2017;542:352–356.

3. Dobie R, Wilson-Kanamori JR, Henderson BEP, Smith JR, Matchett KP, Portman JR, Wallenborg K, Picelli S, Zagorska A, Pendem SV, Hudson TE, Wu MM, Budas GR, Breckenridge DG, Harrison EM, Mole DJ, Wigmore SJ, Ramachandran P, Ponting CP, Teichmann SA, Marioni JC, Henderson NC. Single-cell transcriptomics uncovers zonation of function in the mesenchyme during liver fibrosis. Cell Rep 2019;29:1832–1847.e8.

4. Aizarani N, Saviano A, Sagar, Mailly L, Durand S, Herman JS, Pessaux P, Baumert TF, Grun D. A human liver cell atlas reveals heterogeneity and epithelial progenitors. Nature 2019;572:199–204.

5. MacParland SA, Liu JC, Ma XZ, Innes BT, Bartczak AM, Gage BK, Manuel J, Khuu N, Echeverri J, Linares I, Gupta R, Cheng ML, Liu LY, Camat D, Chung SW, Seliga RK, Shao Z, Lee E, Ogawa S, Ogawa M, Wilson MD, Fish JE, Selzner M, Ghanekar A, Grant D, Greig P, Sapisochin G, Selzner N, Winegarden N, Adeyi O, Keller G, Bader GD, McGilvray ID. Single cell RNA sequencing of human liver reveals distinct intrahepatic macrophage populations. Nat Commun 2018;9:4383.

6. Ramachandran P, Dobie R, Wilson-Kanamori JR, Dora EF, Henderson BEP, Luu NT, Portman JR, Matchett KP, Brice M, Marwick JA, Taylor RS, Efremova M, Vento-Tormo R, Carragher NO, Kendall TJ, Fallowfield JA, Harrison EM, Mole DJ, Wigmore SJ, Newsome PN, Weston CJ, Iredale JP, Tacke F, Pollard JW, Ponting CP, Marioni JC, Teichmann SA, Henderson NC. Resolving the fibrotic niche of human liver cirrhosis at single-cell level. Nature 2019;575:512–518.

7. Shutter JR, Scully S, Fan W, Richards WG, Kitajewski J, Deblandre GA, Kintner CR, Stark KL. Dll4, a novel Notch ligand expressed in arterial endothelium. Genes Dev 2000;14:1313–1318.

8. Wang B, Zhao L, Fish M, Logan CY, Nusse R. Self-renewing diploid Axin2(+) cells fuel homeostatic renewal of the liver. Nature 2015;524:180–185.

9. Rocha AS, Vidal V, Mertz M, Kendall TJ, Charlet A, Okamoto H, Schedl A. The angiocrine factor Rspondin3 is a key determinant of liver zonation. Cell Rep 2015;13:1757–1764.

10. Kalucka J, de Rooij L, Goveia J, Rohlenova K, Dumas SJ, Meta E, Conchinha NV, Taverna F, Teuwen LA, Veys K, Garcia-Caballero M, Khan S, Geldhof V, Sokol L, Chen R, Treps L, Borri M, de Zeeuw P, Dubois C, Karakach TK,

Falkenberg KD, Parys M, Yin X, Vinckier S, Du Y, Fenton RA, Schoonjans L, Dewerchin M, Eelen G, Thienpont B, Lin L, Bolund L, Li X, Luo Y, Carmeliet P. Single-cell transcriptome atlas of murine endothelial cells. Cell 2020;180:764–779.e20.

11. Chen L, Gu T, Li B, Li F, Ma Z, Zhang Q, Cai X, Lu L. Delta-like ligand 4/DLL4 regulates the capillarization of liver sinusoidal endothelial cell and liver fibrogenesis. Biochim Biophys Acta Mol Cell Res 2019; 1866:1663–1675.

12. Xu M, Xu HH, Lin Y, Sun X, Wang LJ, Fang ZP, Su XH, Liang XJ, Hu Y, Liu ZM, Cheng Y, Wei Y, Li J, Li L, Liu HJ, Cheng Z, Tang N, Peng C, Li T, Liu T, Qiao L, Wu D, Ding YQ, Zhou WJ. LECT2, a ligand for Tie1, plays a crucial role in liver fibrogenesis. Cell 2019; 178:1478–1492.e20.

13. Xue C, Huang Q, Zhang T, Zhao D, Ma Q, Tian T, Cai X. Matrix stiffness regulates arteriovenous differentiation of endothelial progenitor cells during vasculogenesis in nude mice. Cell Prolif 2019;52:e12557.

14. Mouta Carreira C, Nasser SM, di Tomaso E, Padera TP, Boucher Y, Tomarev SI, Jain RK. LYVE-1 is not restricted to the lymph vessels: expression in normal liver blood sinusoids and down-regulation in human liver cancer and cirrhosis. Cancer Res 2001;61:8079–8084.

15. Wisse E. An electron microscopic study of the fenestrated endothelial lining of rat liver sinusoids. J Ultrastruct Res 1970;31:125–150.

16. Bhunchet E, Fujieda K. Capillarization and venularization of hepatic sinusoids in porcine serum-induced rat liver fibrosis: a mechanism to maintain liver blood flow. Hepatology 1993;18:1450–1458.

17. Horn T, Christoffersen P, Henriksen JH. Alcoholic liver injury: defenestration in noncirrhotic livers–a scanning electron microscopic study. Hepatology 1987;7:77–82.

18. DeLeve LD. Liver sinusoidal endothelial cells in hepatic fibrosis. Hepatology 2015;61:1740–1746.

19. Desroches-Castan A, Tillet E, Ricard N, Ouarne M, Mallet C, Belmudes L, Coute Y, Boillot O, Scoazec JY, Bailly S, Feige JJ. Bone morphogenetic protein 9 Is a paracrine factor controlling liver sinusoidal endothelial cell fenestration and protecting against hepatic fibrosis. Hepatology 2019;70:1392–1408.

20. Scoazec JY, Feldmann G. The cell adhesion molecules of hepatic sinusoidal endothelial cells. J Hepatol 1994; 20:296–300.

21. Connolly MK, Bedrosian AS, Malhotra A, Henning JR, Ibrahim J, Vera V, Cieza-Rubio NE, Hassan BU, Pachter HL, Cohen S, Frey AB, Miller G. In hepatic fibrosis, liver sinusoidal endothelial cells acquire enhanced immunogenicity. J Immunol 2010; 185:2200–2208.

22. Sidney LE, Branch MJ, Dunphy SE, Dua HS, Hopkinson A. Concise review: evidence for CD34 as a common marker for diverse progenitors. Stem Cells 2014;32:1380–1389.

23. Couvelard A, Scoazec JY, Feldmann G. Expression of cell-cell and cell-matrix adhesion proteins by sinusoidal endothelial cells in the normal and cirrhotic human liver. Am J Pathol 1993;143:738–752.

24. Muro H, Shirasawa H, Kosugi I, Nakamura S. Defect of Fc receptors and phenotypical changes in sinusoidal endothelial cells in human liver cirrhosis. Am J Pathol 1993;143:105–120.

25. Xie G, Wang X, Wang L, Wang L, Atkinson RD, Kanel GC, Gaarde WA, Deleve LD. Role of differentiation of liver sinusoidal endothelial cells in progression and regression of hepatic fibrosis in rats. Gastroenterology 2012; 142:918–927.e6.

26. Poisson J, Lemoinne S, Boulanger C, Durand F, Moreau R, Valla D, Rautou PE. Liver sinusoidal endothelial cells: physiology and role in liver diseases. J Hepatol 2017;66:212–227.

27. Cuervo AM, Dice JF. A receptor for the selective uptake and degradation of proteins by lysosomes. Science 1996;273:501–503.

28. Shah V, Haddad FG, Garcia-Cardena G, Frangos JA, Mennone A, Groszmann RJ, Sessa WC. Liver sinusoidal endothelial cells are responsible for nitric oxide modulation of resistance in the hepatic sinusoids. J Clin Invest 1997;100:2923–2930.

29. Iwakiri Y. Endothelial dysfunction in the regulation of cirrhosis and portal hypertension. Liver Int 2012; 32:199–213.

30. Braddock M, Schwachtgen JL, Houston P, Dickson MC, Lee MJ, Campbell CJ. Fluid shear stress modulation of gene expression in endothelial cells. News Physiol Sci 1998;13:241–246.

31. Gracia-Sancho J, Russo L, Garcia-Caldero H, Garcia-Pagan JC, Garcia-Cardena G, Bosch J. Endothelial expression of transcription factor Kruppel-like factor 2 and its vasoprotective target genes in the normal and cirrhotic rat liver. Gut 2011;60:517–524.

32. Shen B, Smith RS Jr, Hsu YT, Chao L, Chao J. Kruppel-like factor 4 is a novel mediator of Kallistatin in inhibiting endothelial inflammation via increased endothelial nitric-oxide synthase expression. J Biol Chem 2009; 284:35471–35478.

33. Angus PW. Role of endothelin in systemic and portal resistance in cirrhosis. Gut 2006;55:1230–1232.

34. Ribera J, Pauta M, Melgar-Lesmes P, Cordoba B, Bosch A, Calvo M, Rodrigo-Torres D, Sancho-Bru P, Mira A, Jimenez W, Morales-Ruiz M. A small population of liver endothelial cells undergoes endothelial-to-mesenchymal transition in response to chronic liver injury. Am J Physiol Gastrointest Liver Physiol 2017; 313:G492–G504.

35. Dufton NP, Peghaire CR, Osuna-Almagro L, Raimondi C, Kalna V, Chuahan A, Webb G, Yang Y, Birdsey GM, Lalor P, Mason JC, Adams DH, Randi AM. Dynamic regulation of canonical TGFbeta signalling by endothelial transcription factor ERG protects from liver fibrogenesis. Nat Commun 2017;8:895.

36. Li Z, Chen B, Dong W, Kong M, Fan Z, Yu L, Wu D, Lu J, Xu Y. MKL1 promotes endothelial-to-mesenchymal transition and liver fibrosis by activating TWIST1 transcription. Cell Death Dis 2019;10:899.

37. Ganesan LP, Mohanty S, Kim J, Clark KR, Robinson JM, Anderson CL. Rapid and efficient clearance of blood-

borne virus by liver sinusoidal endothelium. PLoS Pathog 2011;7:e1002281.

38. Malovic I, Sorensen KK, Elvevold KH, Nedredal GI, Paulsen S, Erofeev AV, Smedsrod BH, McCourt PA. The mannose receptor on murine liver sinusoidal endothelial cells is the main denatured collagen clearance receptor. Hepatology 2007;45:1454–1461.

39. Hansen B, Longati P, Elvevold K, Nedredal GI, Schledzewski K, Olsen R, Falkowski M, Kzhyshkowska J, Carlsson F, Johansson S, Smedsrod B, Goerdt S, Johansson S, McCourt P. Stabilin-1 and stabilin-2 are both directed into the early endocytic pathway in hepatic sinusoidal endothelium via interactions with clathrin/AP-2, independent of ligand binding. Exp Cell Res 2005;303:160–173.

40. Elvevold K, Simon-Santamaria J, Hasvold H, McCourt P, Smedsrod B, Sorensen KK. Liver sinusoidal endothelial cells depend on mannose receptor-mediated recruitment of lysosomal enzymes for normal degradation capacity. Hepatology 2008;48:2007–2015.

41. Ganesan LP, Kim J, Wu Y, Mohanty S, Phillips GS, Birmingham DJ, Robinson JM, Anderson CL. FcgammaRIIb on liver sinusoidal endothelium clears small immune complexes. J Immunol 2012;189:4981–4988.

42. Ohmura T, Enomoto K, Satoh H, Sawada N, Mori M. Establishment of a novel monoclonal antibody, SE-1, which specifically reacts with rat hepatic sinusoidal endothelial cells. J Histochem Cytochem 1993; 41:1253–1257.

43. Yokomori H, Oda M, Yasogawa Y, Nishi Y, Ogi M, Takahashi M, Ishii H. Enhanced expression of endothelin B receptor at protein and gene levels in human cirrhotic liver. Am J Pathol 2001;159:1353–1362.

44. Iglarz M, Steiner P, Wanner D, Rey M, Hess P, Clozel M. Vascular effects of endothelin receptor antagonists depends on their selectivity for ETA versus ETB receptors and on the functionality of endothelial ETB receptors. J Cardiovasc Pharmacol 2015;66:332–337.

45. Bohm F, Ahlborg G, Johansson BL, Hansson LO, Pernow J. Combined endothelin receptor blockade evokes enhanced vasodilatation in patients with atherosclerosis. Arterioscler Thromb Vasc Biol 2002; 22:674–679.

46. Cardillo C, Campia U, Bryant MB, Panza JA. Increased activity of endogenous endothelin in patients with type II diabetes mellitus. Circulation 2002;106:1783–1787.

47. Rafnsson A, Matic LP, Lengquist M, Mahdi A, Shemyakin A, Paulsson-Berne G, Hansson GK, Gabrielsen A, Hedin U, Yang J, Pernow J. Endothelin-1 increases expression and activity of arginase 2 via ETB receptors and is co-expressed with arginase 2 in human atherosclerotic plaques. Atherosclerosis 2020; 292:215–223.

48. Morawietz H, Duerrschmidt N, Niemann B, Galle J, Sawamura T, Holtz J. Induction of the oxLDL receptor LOX-1 by endothelin-1 in human endothelial cells. Biochem Biophys Res Commun 2001;284:961–965.

49. Feng HQ, Weymouth ND, Rockey DC. Endothelin antagonism in portal hypertensive mice: implications for endothelin receptor-specific signaling in liver disease.

50. Am J Physiol Gastrointest Liver Physiol 2009; 297:G27–G33.

50. Pardali E, Sanchez-Duffhues G, Gomez-Puerto MC, Ten Dijke P. TGF-beta-induced endothelial-mesenchymal transition in fibrotic diseases. Int J Mol Sci 2017;18:2157.

51. Zeisberg EM, Tarnavski O, Zeisberg M, Dorfman AL, McMullen JR, Gustafsson E, Chandraker A, Yuan X, Pu WT, Roberts AB, Neilson EG, Sayegh MH, Izumo S, Kalluri R. Endothelial-to-mesenchymal transition contributes to cardiac fibrosis. Nat Med 2007;13:952–961.

52. Zeisberg EM, Potenta SE, Sugimoto H, Zeisberg M, Kalluri R. Fibroblasts in kidney fibrosis emerge via endothelial-to-mesenchymal transition. J Am Soc Nephrol 2008;19:2282–2287.

53. Pitulescu ME, Schmidt I, Benedito R, Adams RH. Inducible gene targeting in the neonatal vasculature and analysis of retinal angiogenesis in mice. Nat Protoc 2010; 5:1518–1534.

54. Loureiro-Silva MR, Iwakiri Y, Abraldes JG, Haq O, Groszmann RJ. Increased phosphodiesterase-5 expression is involved in the decreased vasodilator response to nitric oxide in cirrhotic rat livers. J Hepatol 2006; 44:886–893.

55. Trauner M, Arrese M, Soroka CJ, Ananthanarayanan M, Koeppel TA, Schlosser SF, Suchy FJ, Keppler D, Boyer JL. The rat canalicular conjugate export pump (Mrp2) is down-regulated in intrahepatic and obstructive cholestasis. Gastroenterology 1997;113:255–264.

56. Cabral F, Miller CM, Kudrna KM, Hass BE, Daubendiek JG, Kellar BM, Harris EN. Purification of hepatocytes and sinusoidal endothelial cells from mouse liver perfusion. J Vis Exp 2018;132:56993.

57. Yu G, Wang LG, Han Y, He QY. clusterProfiler: an R package for comparing biological themes among gene clusters. OMICS 2012;16:284–287.

58. Miller CN, Hartigan-O'Connor DJ, Lee MS, Laidlaw G, Cornelissen IP, Matloubian M, Coughlin SR, McDonald DM, McCune JM. IL-7 production in murine lymphatic endothelial cells and induction in the setting of peripheral lymphopenia. Int Immunol 2013;25:471–483.

Correspondence
Address correspondence to: Yasuko Iwakiri, PhD, Section of Digestive Diseases, Department of Internal Medicine, Yale School of Medicine, TAC S223B, 333 Cedar Street, New Haven, Connecticut 06520. e-mail: yasuko.iwakiri@yale.edu; fax: (203) 785-7273.